

Sky surveys and deep fields of ground-based and space telescopes

V.P. Reshetnikov

Astronomical Institute of St.Petersburg State University, Universitetskii pr. 28, Petrodvoretz, 198504 Russia; resh@astro.spbu.ru

Selected results obtained in major observational sky surveys (DSS, 2MASS, 2dF, SDSS) and deep field observations (HDF, GOODS, HUDF, etc.) are reviewed. Modern surveys provide information on the characteristics and space distribution of millions of galaxies. Deep fields allow one to study galaxies at the stage of formation and to trace their evolution over billions of years. The wealth of observational data is altering the face of modern astronomy: the formulation of problems and their solutions are changing and all the previous knowledge, from planetary studies in the solar system to the most distant galaxies and quasars, is being revised.

1. Introduction

People have always tried to understand the surrounding world. By now, many figures and plans have been collected showing the way people have tried to systematize their knowledge, from geographic maps to pure speculative scheme of the Universe ([1], Fig. 1).

For a very long time, humankind included numerous “fixed” stars, planets, the Sun, and the Moon into its sphere of interests. Probably, the first systematic survey of all that is visible by the naked eye was performed by Hipparchus in the 2nd century BC. He drew up a catalog including about 850 stars. After almost two thousand years, at the end of the 18th century, French astronomer Charles Messier published the first catalog including not stars but stellar clusters and nebulae. As we know, about a third of these nebulae are extragalactic bodies – external galaxies. However, Messier was not interested in the dim fuzzy spots he discovered. He was primarily interested in comets and compiled this catalog in order to distinguish comets from fixed nebulae.

William Herschel (1738-1822, “Coelorum perrupit claustra”) was the first to formulate the problem of global sky surveys to study the structure and evolution of the world outside the solar system [2]. To survey stars in the sky, he applied the original method of “star gauging” (counting the number of stars in selected sky areas¹) and statistical data analysis. This allowed him to establish the general shape of our Galaxy and to estimate correctly its oblateness ($\sim 1/5$). Another great merit of Herschel was the first systematic survey of faint nebulae and an attempt to

establish regularities in their large-scale distribution. He discovered more than 2.5 thousand nebulae and star clusters, of which 80% are other galaxies. Herschel was first to attempt to estimate the size of dim nebulae and to measure their distance. His very approximate estimations gave rise to a picture of the Universe where the Milky Way is an ordinary stellar system of an infinite number of other galaxies. In the 19th century, his son John Herschel (1792-1871) continued searches for and studies of ‘milky nebulae.’ John Herschel expanded his study to the southern hemisphere, doubled the number of known faint nebulae, and continued studying their distribution in the sky.

The photographic process discovered in the middle of the 19th century allowed astronomers to abandon visual observations and to proceed to photographic sky surveys. At the end of the 19th century, E. Barnard (1857-1923) started systematic photographic observations of the sky and performed the first photographic survey of the Milky Way. Studies of the structure and dynamics of our Galaxy greatly benefited from the plan of ‘selected areas’ by J. Kapteyn (1851-1922). To execute this project, Kapteyn called upon astronomers from across the world to carry out photographic observations and to carefully study stars (including counting and measuring apparent magnitudes, proper motions, etc.) in 206 areas evenly distributed over the sky. This plan clearly demonstrated the fruitfulness of international collaboration in solving laborious observational problems and anticipated some features of big modern observational projects.

After E. Hubble (1889-1953) discovered the extragalactic nature of faint nebulae, it became clear that the Universe is much larger than had previously been thought. In order to study the large-scale structure of the Universe and to understand the nature, origin, and evolution of its

¹ This was one of a few cases where an astronomer, in full agreement with the commonplace opinion about his kind of work, actually “counted stars” by looking through a telescope.

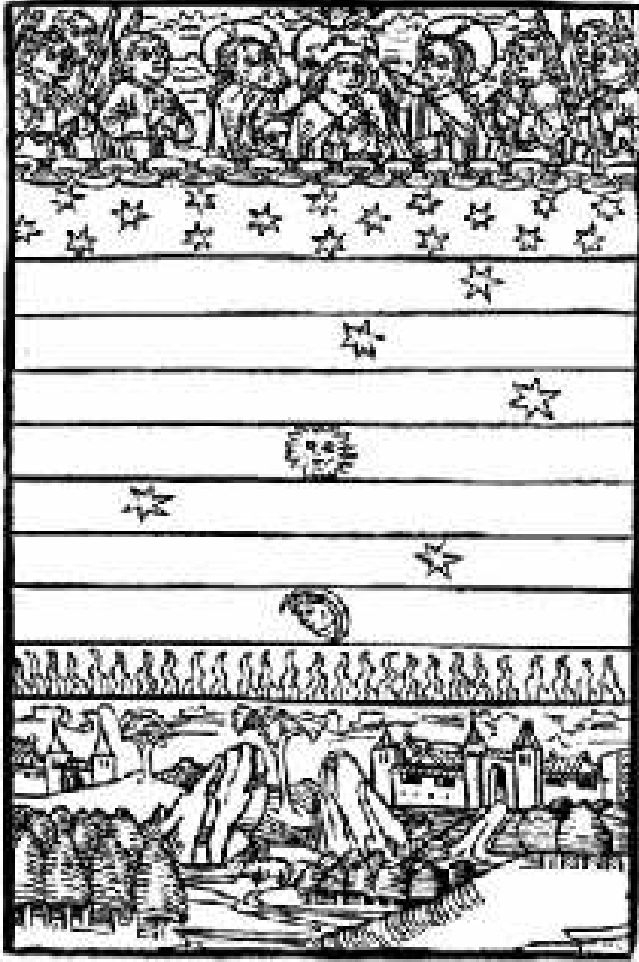


Fig. 1. The structure of the Universe according to concepts of the middle of the 14th century [1]. At the bottom, the earth, water, air, and everything created from them are shown. The horizontal layers from bottom to top show: the sphere of fire, the sphere of seven planets' (the Moon, Mercury, Venus, the Sun, Mars, Jupiter, Saturn), the sphere of fixed stars, and divine heavens totally screened from observation by opaque clouds.

principal 'bricks' – galaxies, extensive sets of extragalactic studies had to be compiled and analyzed. This work was started by Hubble himself (see, e.g., [3]), as well as by other astronomers (Shapley, Ames, Humason, Lundmark, Bok, etc.).

At the end of the 1920s – beginning of the 1930s, Hubble performed a laborious survey of more than 40,000 galaxies in 1,283 areas located in both celestial hemispheres [4]. The main results of Hubble's work can be summarized as follows: the number of galaxies continues to grow up to the limiting magnitude of the survey; this growth is in quantitative agreement with a homogeneous distribution of galaxies in space (later, Hubble discovered that integral counts of fainter galaxies increase more slowly than was expected for their homogeneous distribution); there is a strong dependence of the observed number of galaxies per unit area of the sky on the galactic lati-

tude (due to Galactic extinction); it is the logarithm of the number of galaxies per square degree (N) and not the number N itself that, after reducing all plates to standard conditions, follows a Gaussian distribution. This last discovery was one of the first indications that galaxies tend to 'crowd' [5]. Hubble's results strongly differed from star counts: in counting stars, we reach the boundaries of our stellar system, while observations of galaxies do not show the presence of a boundary of the extragalactic world.

During the entire subsequent history of the 20th century, the main achievements in sky surveys and deep studies of selected areas were due to 'technological' successes, such as the use of new big and specialized telescopes, increasingly sensitive photo emulsions, and then CCD matrices and computers, the elaboration of multi-object spectroscopy, etc. Each such a 'technological' step has led to ever deeper penetration into the Universe.

The invention of a new telescopic system, the wide-field reflector, by Estonian optician Bernhard Schmidt (1879-1935) was one of the most important stages in the development of the observational technique. A correcting plate mounted in front of a reflector's objective allows compensating for most aberrations of the main mirror. This opens the possibility to construct candlepower telescopes with a wide ($\sim 10^\circ$) undistorted field of view. The best known Schmidt telescope (the correction plate diameter is 122 cm, the diameter of the objective is 183 cm) is installed at the Mount Palomar Observatory in California. Its field of view is 6.6° . In 1950-1958, this telescope was used to carry out the famous Palomar Sky Survey (see below). The biggest Schmidt telescope (the correction plate diameter is 137 cm, the diameter of the objective is 200 cm) is installed near Jena in Germany. The biggest telescope of this kind on the territory of the former Soviet Union operates at Byurakan Observatory (Armenia) (the correction plate diameter is 102 cm, the diameter of the objective is 132 cm, the field of view is 4°). The Byurakan Schmidt telescope was used to carry out the well-known survey of galaxies with ultraviolet excess (the so-called Markarian galaxies).

In the last 10-15 years, several international projects have been carried out that distinctively changed the aspect of modern astronomy. Observational data on the structure of our and other galaxies were increased by dozens and hundreds of times. For the first time, it became possible to study the evolution of galaxies and their large-scale structure starting almost from the moment of their formation until now. There are statements that a 'golden age' of studies of galaxy formation and evolution has begun. The general feeling among astronomers and physicists (especially theoreticians) is partially characterized by the title of a colloquium that took place at Caltech several years ago: "Galaxy formation: End of the Road!" [6].

Time will tell how justified such optimism is, but undoubtedly extragalactic astronomy and observational cosmology are in a period now that can possibly be compared only with the 1920s, when the first galaxies were identified

and the expansion of the Universe was discovered. In this paper, I attempt to briefly review selected observational projects of the last years. In view of the immense observational data, I restrict myself to *optical* and *extragalactic* surveys.

Throughout the review, I use a cosmological model with $\Omega_m = 0.3$, $\Omega_\Lambda = 0.7$, and $H_0 = 70$ km/s/Mpc.

2. General characteristics of surveys and deep fields

Sky surveys and so-called ‘deep fields’ represent different strategies for studying extraterrestrial objects. There are no strict criteria distinguishing deep studies of selected areas and surveys. Guided by the characteristics of the most known projects, the following empirical definitions can be proposed.

Sky surveys include projects performing photometric and/or spectral observations of a significant fraction of the sky (the total coverage $\geq 10^4$ sq. deg.). The effective depth of surveys is $z \sim 0.1$ (here and below, z denotes redshift) or several hundred megaparsecs (Mpc). Modern sky surveys are carried out over several years by using, as a rule, middle-size specialized telescopes.

Deep fields relate to projects devoted to a detailed exploration of relatively small sky areas (the characteristic field coverage is $10^{-3} - 10^1$ sq. deg.). Fields are much deeper ($z \geq 0.5$) compared to surveys and observations are performed with large telescopes. The typical exposures of a deep field are $10^{-3} - 10^{-1}$ year.

‘Integral’ characteristics of some contemporary observational projects, many of which are discussed in detail below, are plotted in Fig. 2 in the plane $B - \lg S$ (a) and $B - \lg(N/S)$ (b), where B is the limiting magnitude of galaxies found in a survey or within a field in the B filter², S is the area on the sky (in square degrees), and N is the number of galaxies found.

Figure 2 clearly illustrates the formal distinction introduced above between surveys and deep fields: the characteristics of modern projects are concentrated mostly in regions with $S \leq 1$ sq. deg. and $S \geq 1000$ sq. deg. This, of course, must be a temporary situation, and one can imagine a not-too-remote future when large fully robotic telescopes will measure galaxies with $B \approx 25^m - 30^m$ over most of the sky (the top right in Fig. 2a).

The dashed curve in Fig. 2a shows the simplest observational strategy with $E_{lim}/S = \text{const}$ (E_{lim} is the illumination from the faintest objects detected). Such a dependence between E_{lim} and the area can be expected if observations are carried out using one instrument with a fixed field of view over a fixed total observation time. Big modern projects with $B \geq 18^m$ show a steeper dependence in the $B - \lg S$ plane, biased by the observations being made with larger telescopes with a narrower, on average, field of view.

² In some cases, the limiting magnitude value was approximately estimated from data in other color bands.

Figure 2b shows the surface density of galaxies (the number of galaxies per square degree) as a function of the limiting apparent magnitude of the project. (It should be borne in mind that the limiting magnitude values are determined differently by different authors.) This figure demonstrates that the number of galaxies per square unit continuously increases up to $B \approx 30^m$. The old result obtained by Hubble [7] is also clearly seen: the observed number of galaxies increases with the limiting magnitude more slowly than is expected for a homogeneous distribution in Euclidean space (the dotted line in Fig. 2b). The reasons for such behavior of galactic counts are the expansion of the Universe and the evolution of galaxies with time.

Figure 2b allows one to evaluate the number of galaxies available for observation in the Universe. It can be seen that the number of galaxies with $B \leq 30^m$ is about 1.5×10^6 /sq. deg. (i.e., one galaxy per each $3'' \times 3''$ square). Hence, the total number of galaxies with $B \leq 30^m$ is $\sim 10^{11}$.

The actual volume of the Universe probed in a survey or a deep field is determined, in addition to the deepness and area, by a selection function – a set of criteria used to select the objects. The most widespread methods of object selection are as follows [8]:

(1) *Selection of all objects with a density flux above a fixed threshold.* The detection limit is set, as a rule, in fractions of the standard deviation of the night sky brightness fluctuations. The simplicity of this method allows a simple estimation of the space volume probed. The maximum redshift (z_{max}) at which an object with the proper (rest-frame) luminosity L is still detectable at a given threshold E_{lim} can be inferred from the relation $L = E_{lim} 4\pi D_L^2$, where D_L is the photometric distance depending on z_{max} . Then, the volume of a survey (deep field) is

$$V_{max}(z, L) = S \int_0^{z_{max}} Q(z, \Omega_m, \Omega_\Lambda) dz,$$

where the function Q depends on the cosmological model assumed (Ω_m and Ω_Λ are the relative contributions of matter and vacuum energy to the total density of the Universe.)

It should be noted that in practice, the selection is made using not the observed flux densities but, to a greater extent, the surface brightness of galaxies. For example, an object is often believed to be detected if its flux in several neighboring pixels in the CCD-image exceeds background fluctuations by several times. Naturally, this procedure is biased in favor of objects with a sufficiently high surface brightness.

(2) *Selection by color indices.* This method accounts for not only the observed flux but also the color indices, i.e., the relative energy distribution in the galactic spectra. It is widely applied to find the most distant galaxies, because their spectra show a distinctive break near the Lyman limit (912 Å) [9]. In the past, this approach proved to be extremely effective in discovering galaxies with ultra-violet excess (the Markarian galaxies) and galaxies with

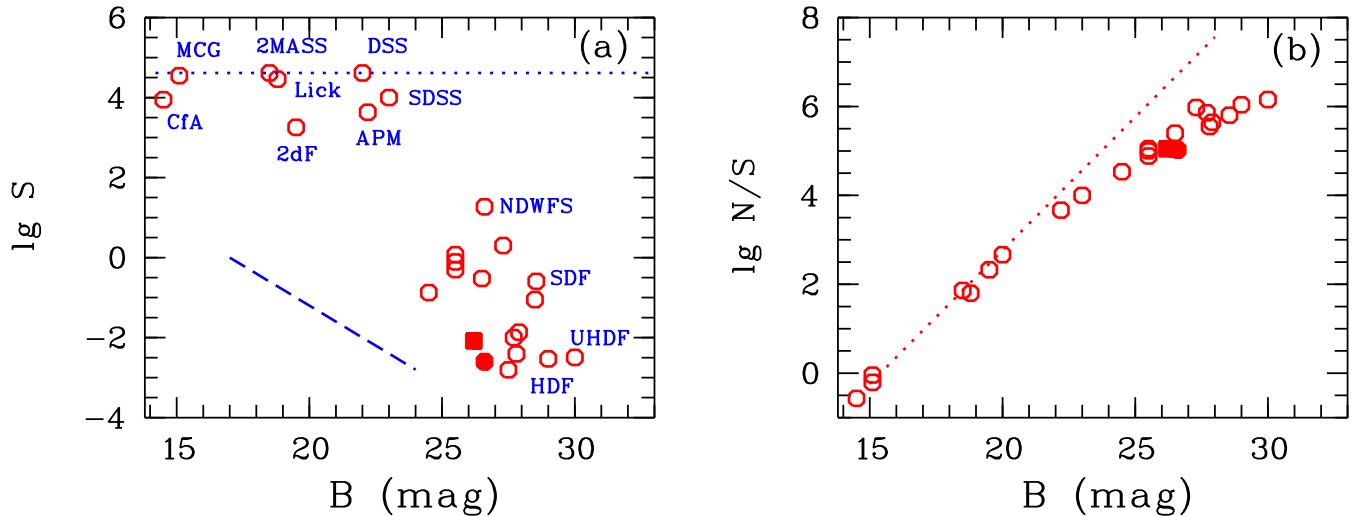


Fig. 2. Characteristics of the main modern observational projects. The horizontal dotted line in Fig. (a) shows the total area of the sky. The black square and circle mark works performed with the 6-m SAO RAN telescope (see Section 4.9).

active nuclei (see, e.g., [10]). The calculation of the selection function and, correspondingly, the space volume probed by observations using this method is strongly dependent on the precise knowledge of the spectral energy distribution in the objects under study.

(3) *Selection by narrow-band observations.* The essence of this method is the selection of galaxies that show an excess when observed in narrow-band filters with respect to broad-band ones. This method is used to search for objects with emission lines (star-forming galaxies, active galactic nuclei). Observations are performed with narrow filters cutting spectral ranges $\leq 100 \text{ \AA}$ (to increase the contrast of the emission object against the sky background) centered on the wavelength (for example, $\text{Ly}\alpha$) corrected for the expected redshift of a distant object. Clearly, in this case, the selection function is determined by the equivalent width of the emission line in the galaxy.

A shortcoming of this approach is that galaxies are searched for only in a very narrow interval of redshifts z and samples obtained in this way are relatively small. In addition, only a small fraction of all galaxies from this redshift interval is selected (namely, those that show a large equivalent width of emission lines). These reservations restrict obtaining statistically significant results on the general features of distant galaxies.

After the above comments, we turn to describing selected projects. Projects similar to those described below are currently being carried out at many observatories. Many dozens of papers discussing the results of both new and old surveys and deep fields are published each year. This diversity of projects can be quite confusing (especially because many projects have similar abbreviations). I therefore describe only the principal projects playing an outstanding role in modern astronomy.

The main goal of the following ‘technical’ description (Sections 3 and 4) is to give the reader a flavor of the very

rapidly growing observational base of modern astronomy. A distinctive feature of the last years is that the observational data obtained are freely available for the scientific community via the corresponding www pages.

3. Sky surveys

3.1. Photographic surveys

Photographic surveys performed with Schmidt telescopes [11] had a great impact on the development of astronomy. In the 1950s, a photographic survey of the sky available for observations from California ($\delta > -33^\circ$) was performed using the 1.2-m telescope of the Palomar Observatory. Almost a thousand plates $6.^\circ 5 \times 6.^\circ 5$ each were obtained in the blue and red spectral bands. Copies of the Palomar sky survey (in the form of glass or printed copies of the plates) were spread over most astronomical institutes in the world and played a very important role in the development of all fields of astronomy, from solar system studies to remote galaxies and quasars [11]. Objects down to $B \sim 20^m$ can be distinguished in the Palomar prints, and the structure of tens of thousands of galaxies with $B \leq 15^m$ can be studied. In particular, based on the Palomar survey (its official name is the Palomar Observatory Sky Survey I, or POSS-I), catalogs of galaxies by Zwicky [12] and Vorontsov-Velyaminov (MCG in Fig. 2a) [13] were compiled. It is by inspecting copies of this survey that systematic studies of galaxies, from interacting [14] and double ones [15] to galaxy clusters [12, 16], began.

In the 1970s, the success of the Palomar survey stimulated carrying out similar surveys of the southern sky by the 1.2-m British Schmidt telescope (the Anglo-Australian Observatory (AAO), Australia) and the 1.0-m Schmidt telescope of the European Southern Observatory in Chile. Due to great progress in constructing telescopes

and improving quality of photographic emulsions, the limiting apparent magnitude of these surveys (ESO/SERC) is by about $1.^m5$ smaller than in POSS-I. This, in turn, initiated, at the end of the 1980s, re-surveying the northern sky with the modified Palomar Schmidt telescope using improved emulsions, but this time with three filters, including the near infrared band centered on $\lambda_{eff} \approx 8500$ Å. This survey was named POSS-II [17]. The limiting magnitude in POSS-II for star-like objects is $B \approx 22.^m5$.

One photographic plate taken by a large Schmidt telescope can have 10^5 – 10^6 images of stars and galaxies. This restricted earlier works by visual inspection of only small areas of the original plates. The effective reading of information from the Schmidt plates became possible only after high-speed measuring machines were designed that allowed image digitizing and subsequent computer processing. It is in this way that the first digital sky surveys APM and DSS appeared at the beginning of the 1990s.

3.2. APM

In this project, the microdensitometer APM (Automatic Plate Measuring machine) in Cambridge, England, was used to scan 185 plates (the scan step was $0.''5$) obtained with the 1.2-m Schmidt telescope of the Anglo–Australian Observatory (Australia) near the southern galactic pole [18]. The plates cover ~ 4300 sq. deg. on the sky. Around 20×10^6 objects with $B \leq 22^m$ were discovered on these plates. For each object, the coordinates, apparent magnitude, and a dozen other parameters characterizing the brightness distribution and shape were determined. By analyzing photometric brightness profiles, the objects were classified to form a virtually complete sample of extragalactic objects containing $\sim 2 \times 10^6$ galaxies with $B \leq 20.^m5$.

The galaxy distribution of the APM survey over an area of $\sim 50^\circ \times 100^\circ$ is shown in Fig. 3. Obviously, the projected galaxy distribution is far from being homogeneous. Figure 3 clearly shows the presence of regions with an enhanced and low concentration of galaxies and elongated structures. On the basis of the APM survey, some important studies of the large-scale distribution of galaxies were carried out (see, e.g., [19]) and the first objective catalog of galaxy clusters [20] was compiled.

The results of the APM survey and its extensions (in particular, to the northern hemisphere) were used as the basis for one of the most interesting projects of recent years – the 2dF survey of galactic redshifts (see Section 3.5 below).

In addition to APM, one can note several later projects aimed at scanning the Palomar and ESO/SERC plates: for example, APS (USA) [21] and COSMOS and SuperCOSMOS (England) [22, 23]. These surveys are distinguished by a large sky coverage and using plates in different colors.

3.3. DSS and DPOSS

DSS (Digitized Sky Survey) is the first high-quality and freely available digitized image of *the entire sky* in the optical range. This survey stemmed from the Space Telescope Institute (STScI) project on creating a star catalog that can be used to precisely point the Hubble Space Telescope (HST) to a required object and guide it during observations [24]. To compile such a catalog, the scanning of blue photographic plates of the POSS-I and SERC surveys was initiated. The scan step was $1.''7$. Soon, it was understood that the importance of the digitized images is far beyond the original purpose and it was decided to open them to the wider scientific community. The total amount of the original version of the survey (DSS-I) reached 600 GB and, clearly, such a huge amount of data was not easily transportable at the beginning of the 1990s. However, after specially designed tenfold compression of the data, the survey was fit into 120 CD-ROMs, which have been distributed through the Astronomical Society of the Pacific (USA) starting in 1994 [25]. Later on, free access to DSS-I was open through the web pages of STScI (<http://archive.stsci.edu/dss/>). Now, this survey can be remotely accessed through several sites in the USA and Canada, as well as in some European countries and Japan.

The DSS-II survey was the natural extension of DSS-I using data from POSS-II [26]. The POSS-II plates of the northern sky, as well as the SERC plates and other surveys of the southern sky, were scanned with the step $1.''0$. Plates in three color bands were digitized, which allowed a comparison of sky areas in different spectral bands. The total volume of DSS-II attains ~ 5 TB and remote access to it is available, as a rule, through the same web pages as for DSS-I.

From the very beginning, DSS became one of the most useful and required tools of modern astronomy. It allowed obtaining an image of any area of the sky in several seconds, which strongly facilitated the preparation and planning of observations. Using the DSS images, a great number of papers devoted to study of individual galaxies, galaxy groups, their large-scale distribution and geometrical characteristics, the optical identification of objects observed at other wavelengths, etc. have been published.

The DPOSS project (Digitized Palomar Observatory Sky Survey – <http://dposs.caltech.edu>) is also based on scanning the POSS-II plates in three colors; however, the subsequent data processing and calibration are different from those used in DSS [27]. This survey covers all the northern sky with $\delta > -3^\circ$. Extensive CCD-observations were performed at the Palomar Observatory to provide photometric calibrations of this survey. DPOSS includes a database of images scanned with the step $1.''0$ (~ 3 TB) and several catalogs based on these data. The ultimate goal of DPOSS is the creation of the PNSC catalog (Palomar Norris Sky Catalog) including all objects found in the survey up to the limiting magnitude $B \approx 22^m$. More than a hundred measured parameters will be provided for

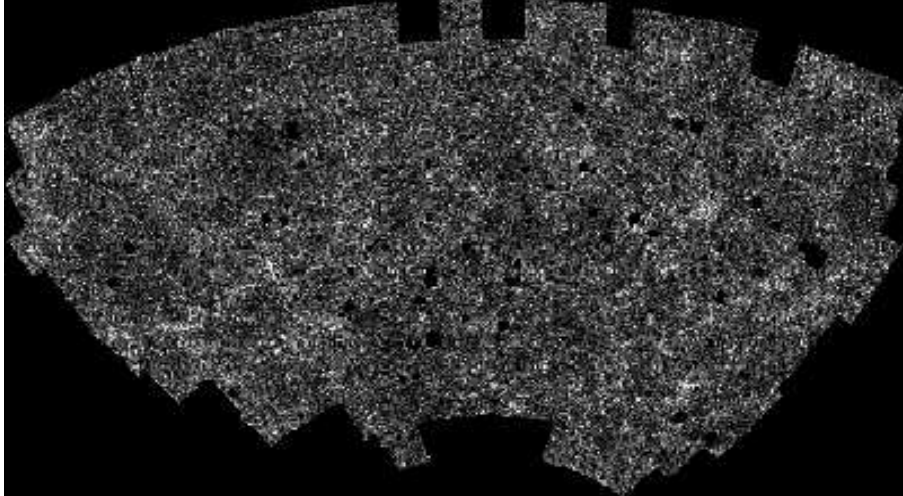


Fig. 3. The visual distribution of APM galaxies.

each source in the catalog, and objects with $B \leq 21^m$ will be classified as stars or galaxies. It is expected that PNSC will provide information on $> 50 \times 10^6$ galaxies (including $\sim 10^5$ quasars) and $> 10^9$ stars.

The surveys mentioned above were based on photographic observations and, naturally, suffer from all the standard shortcomings of photo emulsions, such as low sensitivity, restricted dynamical range, and nonlinearity. All projects (both surveys and deep fields) that we discuss below are truly digital, because CCD detectors are used to perform them.

3.4. 2MASS

One of the best known digital surveys in a wavelength range close to the optical one is 2MASS (Two Micron All Sky Survey), which is the result of the collaborative efforts of the University of Massachusetts and the Infrared Processing and Analysis Center at Caltech (<http://www.ipac.caltech.edu/2mass>). 2MASS is a purely photometric survey covering the whole sky in filters J ($1.25 \mu\text{m}$), H ($1.65 \mu\text{m}$), and K_s ($2.17 \mu\text{m}$) [28]. Observations were carried out from June 1997 to February 2001 with two robotic 1.3-m telescopes in Arizona, USA, and Chile. Each instrument was equipped with a three-channel camera imaging the sky simultaneously in the three spectral bands using 256×256 IR CCD-detectors with the pixel size $2.''0$.

The survey consists of 10 Tbt of images and catalogs of objects. Calibrated images of any area of the sky in the J , H , and K_s -bands are available through several sites (for example, <http://irsa.ipac.caltech.edu/>). An atlas of near-IR images of 864 galaxies has been published [29]. The point source catalog (PSC) lists coordinates and photometric data for about 500 million objects (mostly Milky Way stars). The extended source catalog (XSC) includes data for ~ 1.65 million objects with angular sizes $\geq 10''$ – $15''$ [30]. More than 98% of these objects are galaxies, others are HII regions, stellar clusters, planetary nebulae,

etc. The limiting magnitudes of the extended objects from the XSC are $13.^m5$ (2.9 mJy) and $15.^m0$ (1.6 mJy) in the K_s and J -bands, respectively. Figure 4 shows the distribution of objects from the XSC in galactic coordinates. The letters in this figure mark clusters and superclusters of galaxies, the extended image in the center is the Milky Way stellar disk seen ‘edge-on’ [31].

Over the few years since completion, the 2MASS survey has already greatly impacted the development of astronomy. For example, according to the Astrophysics Data System (ADS: <http://adsabs.harvard.edu>) [32], the number of published papers that used the 2MASS data approached a thousand by the beginning of 2005. The main areas of study benefiting most from using the 2MASS data include the large-scale structure of the Milky Way and distribution of galaxies in the nearby Universe (in the optical range, such studies are strongly restricted by galactic interstellar absorption), as well as searches for and explorations of new types of astronomical objects (for example, low-mass stars, brown dwarfs, ‘red’ quasars, etc.).

3.5. 2dF and 6dF

The 2dF (2 degree Field Galaxy Redshift Survey, or 2dFGRS) represents a spectroscopic survey of $\sim 5\%$ (~ 2000 sq. deg.) of the sky performed by British and Australian astronomers with the 3.9-m telescope of AAO [33, 34]. (The coverage of this survey is rather small to classify it as a survey, according to Section 2, and clearly demonstrates the conditionality of dividing modern projects into surveys and deep fields.) Objects for this survey were sampled using the extended APM source catalog (see Section 3.2) and included galaxies brighter than $B \approx 19.^m5$ near the North and South galactic poles. A specially designed multi-object spectrograph allowing simultaneously obtaining spectra of 400 objects within the 2° field of view was used. Observations included 272 nights in the period between 1997 and 2002.

Fig. 4. The distribution of the 2MASS survey objects in the sky (in galactic coordinates).

The openly accessible results of the project (<http://www.mso.anu.edu.au/2dFGRS/>) include: a photometric catalog of objects selected for spectroscopic studies; a spectroscopic catalog of 245,591 objects listing redshifts z and spectral types (221,414 galaxies in this catalog have reliable redshift measurements); and special software to fetch both fits-files with spectra and subsamples of objects according to selected criteria.

Upon its completion, the 2dF survey became the largest galaxy redshift survey, with the number of measurements exceeding 10^5 for the first time. It allows investigating the three-dimensional large-scale structure of the surrounding Universe with an unprecedented accuracy. The median redshift of the survey is $z = 0.11$, which corresponds to the photometric distance ~ 500 Mpc. As an example, in Fig. 5, we show the distribution of 63,000 galaxies from the survey located within narrow 3° -bands around the north (to the left) and south (to the right) galactic poles [35]. In contrast to Figs 3 and 4, which show the galaxy distribution projected on the sky, this figure plots the galaxy distribution along the line of sight. The decrease in the number of galaxies with increasing z is the result of sampling by apparent magnitude biasing only bright remote galaxies. The principal elements of the large-scale structure of the Universe – clusters and superclusters, filaments, and voids – are clearly seen in Fig. 5.

The 2dF survey plays a major role in modern astronomy as one of the main sources of information on the spatial distribution of galaxies and the density of matter in the Universe. For example, the data from the survey allowed the upper limit of the total mass of the neutrino $m_{\nu, tot} < 1.8$ eV to be derived [36] and, in combination with data on the cosmic microwave background, the values of the main cosmological parameters to be improved [37].

An autonomous subproject within the 2dF is the 2dF QSO Redshift Survey (2QZ), a survey of redshifts of quasars located near the north and south galactic poles (the total coverage is ~ 700 sq. deg.) [38]. The 2QZ contains spectra of 23,338 quasars, 12,292 stars of our Galaxy (including around 2,000 white dwarfs), and 4,558 emission-line galaxies. The data, including photometry, redshifts, and fits-files with spectra, are available via <http://www.2dfquasar.org/>.

The 6dF (6dF Galaxy Survey, or 6dFGS) represents a survey of redshifts and peculiar velocities of galaxies selected mainly from the XSC 2MASS survey catalog (see Section 3.4) [39]. Selecting galaxies in the IR spectral range, where the effect of interstellar absorption inside the Milky Way is much smaller than in the optical range, allows much better studies of the object distribution at low galactic latitudes. The 1.2-m Schmidt telescope of the Anglo–Australian Observatory is used, equipped with a multi-object spectrograph simultaneously taking spectra of 150 objects inside the telescope’s 6-degree field of

view. Redshifts of around 150,000 galaxies are planned to be measured. The survey will cover almost the entire southern sky with $\delta < 0^\circ$ (the survey coverage is ≈ 17000 sq. deg.) and will give detailed information on the distribution of galaxies within the nearby ($z \approx 0.05$) volume of the Universe. At the beginning of 2005, about half of the input galaxy sample was made available (see <http://www.wfau.roe.ac.uk/6dFGS/>).

The principal goal of the 6dF is to study large-scale deviations in the velocity of galaxies from the homogeneous Hubble expansion. The distribution of such deviations provides the unique means to study mass distribution in the Universe independent of the assumptions that galaxies follow the true mass distribution. For about 15,000 early-type galaxies evenly distributed over the southern sky, z -independent distances will be determined using the Fundamental Plane method (the Fundamental Plane is a three-parameter relation between photometric and kinematic characteristics of galaxies, see, e.g., [40]). Then, by comparing these distances with those derived from the observed values of z , it will be possible to estimate the peculiar velocities of galaxies arising due to inhomogeneities in mass distribution. (In this way, the Great Attractor with the mass $\sim 5 \times 10^{16} M_\odot$ in a relatively nearby region of the Universe was found [41]).

3.6. SDSS

The Sloan Digital Sky Survey (<http://www.sdss.org/>) is often referred to as one of the most grandiose astronomical projects in history. Starting at the end of the 1980s, it is being carried out by more than a hundred scientists from the USA, Japan, and some European countries [42, 43].

The purpose of the SDSS is to perform a photometric and spectral study of a quarter (≈ 10000 sq. deg.) of the sky. The survey covers one large area near the Northern Galactic Pole and three bands (with a total coverage of 740 sq. deg.) in the southern hemisphere. Observations are carried out with a specially designed 2.5-m telescope (the modified Ritchey–Chretien system, 3° field of view) in New Mexico (USA). The telescope is equipped with a CCD-camera and a couple of identical multi-object fiber-optic spectrographs to simultaneously take spectra of 640 objects. Auxiliary works are also performed with several other telescopes.

The main goal of the photometric observations is to construct a database for $\sim 10^8$ galaxies and $\sim 10^8$ stars, containing the precise ($\leq 0.''1$) coordinates and photometric and other characteristics. The observations are carried out in five broadband filters in the spectral range from 3500 Å to 9100 Å. The limiting magnitude of the photometric survey is $B \approx 23^m$ for point-like objects.

The spectral observations should provide spectra of about 10^6 galaxies, 10^5 quasars, and 10^5 stars selected

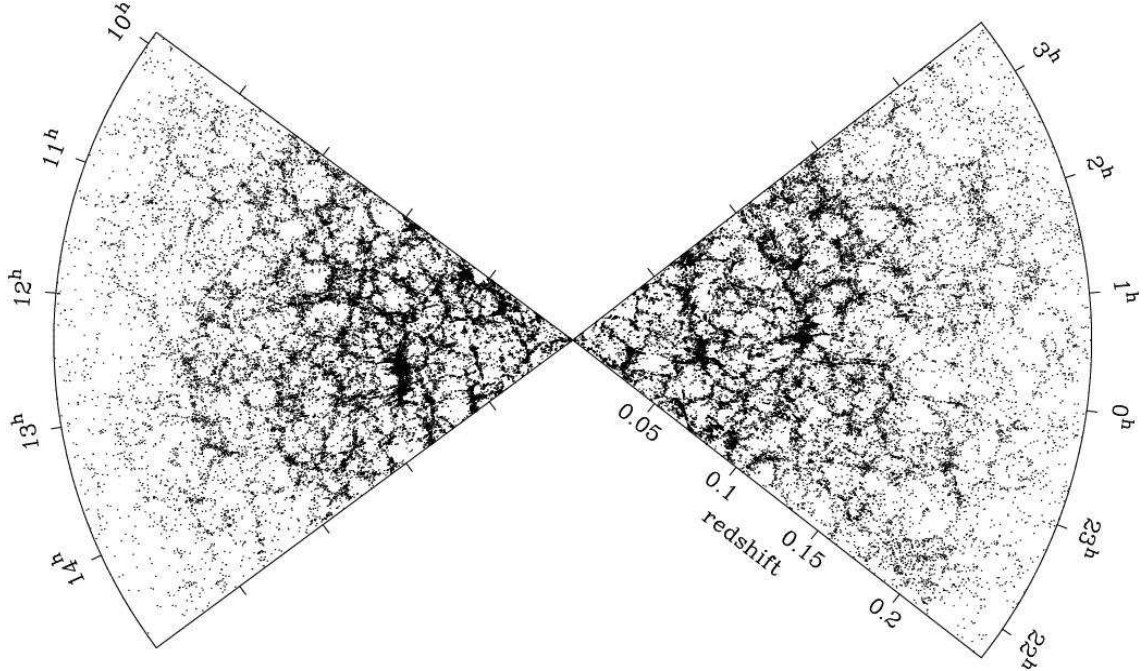


Fig. 5. The distribution of galaxies in the 2dF survey field.

from the photometric survey. Two samples of galaxies have been selected: $\sim 900,000$ galaxies with $B \leq 19^m$ and $\sim 100,000$ objects with large color indices (‘red’ galaxies) and $B \leq 20.^m5$. The quasar candidates are selected using the observed color indices. Stellar-like objects with radio emission are also included in the quasar candidate sample.

Systematic observations for this project started in April 2000 and are to be completed by summer 2005. In the course of the observations, the processed data have become available via the web pages of the survey. By the beginning of 2005, around half of the survey was made available. These data include ~ 6 TB of images, the photometric and astrometric catalogs for 1.41×10^8 objects, and the spectra of 528,640 objects, including 374,767 galaxies, 51,027 quasars, and 71,174 stars [44]. The final results of the SDSS will be presented in 2006.

The SDSS is not yet completed, but a great number of papers (more than a thousand, according to ADS) have already been published. These studies include all fields of optical astronomy, from asteroids (more than several dozen thousand of them have been already discovered by the SDSS) to quasars (quasar redshifts measured in the survey first exceeded the $z = 6$ barrier) [45]. The SDSS and 2dF data increased by hundreds of times the observational information on the structure, spectral characteristics, and spatial distribution of galaxies in the nearby ($z \leq 0.2$) volume of the Universe. At present, almost all characteristics of galaxies known earlier are being revised and improved. This relates in particular to their spatial distribution, the luminosity function, and the dependence of galactic properties and the star formation rate on the environment (see Section 5 below).

4. Deep fields

This section describes some remarkable projects to study relatively small ultra-deep areas – the deep fields (see the lower right corner in Fig. 2a). I will restrict myself to works carried out in the last ten years. Earlier papers are referenced in reviews by Koo and Kron [46], Sandage [47], and Ellis [48].

4.1. WHDF

The WHDF (William Herschel Deep Field) is the deepest ground-based image of a small area taken with a middle-class telescope. The $7' \times 7'$ patch of sky centered on $\alpha(2000) = 00^h 22^m 33^s$ and $\delta(2000) = +00^\circ 21'$ was imaged in 1994–1997 with the 4.2-m William Herschel telescope (the Roque de Los Muchachos Observatory, Spain) [49]. Several dozen thousand CCD-frames were obtained in each of four filters (U , B , R , and I) with the respective total exposure time 34, 28, 8, and 5 h. A careful processing and summing-up of frames enabled reaching the $B \approx 28^m$ limiting magnitude for unresolved objects. The number of galaxies discovered in the WHDF is around six thousand. This field was later imaged in the IR bands by other telescopes.

The results of the WHDF studies have been used to analyze the dependence of the number of galaxies on their apparent magnitude (this provides information on the early cosmological evolution of galaxies), to determine the surface (angular) correlation function of galaxies, and to select the most distant objects by using color indices (see Section 2) [49, 50].

4.2. HDF

The deep fields of the HST [their standard names are the Hubble Deep Field North (HDF-N) and Hubble Deep Field South (HDF-S)] are likely to be the most well-studied patches of the sky. Their exploration has led to some important discoveries on the structure and evolution of distant galaxies [51].

Observations with the HST (the diameter of the main mirror is 2.4 m, the Ritchey Chretien system) in the first half of the 1990s demonstrated that this instrument resolves the structure of distant galaxies and these galaxies look different than those at $z \approx 0$. The idea emerged to use some free time at the discretion of the STScI director (at that time, Robert Williams) to obtain an unprecedented deep image of one typical area at high galactic latitudes [52]. The area was very carefully selected: the interstellar absorption in the Milky Way in its direction had to be small, the area should not have had very bright (in all spectral bands) objects, no relatively close galaxy clusters should have been present, etc. As a result, a region of the sky in Ursa Major was selected.

Observations of this northern area (HDF-N) were carried out in December 1995 with the WFPC-2 (Wide-Field Planetary Camera 2) in four broadband filters centered on 3000 Å (filter F300W), 4500 Å (F450W), 6060 Å (F606W), and 8140 Å (F814W). From fifty to a hundred individual frames were taken, with each frame being taken at a slightly displaced position of the telescope (such that one object fell onto different elements of the CCD matrix). Such a dithering technique allowed obviating the detector's defects and constructing integral deep field images with the step 0."04, which is smaller than the matrix pixel size. The HDF-N covers about 5.3 sq. min., and the field has a nonrectangular shape. The total exposure time in each filter amounted to one to almost two days. The HDF-N was later observed in the near IR bands.

In mid-January of 1996, immediately after primary data processing, the deep field images were open to access through the STScI web-pages (<http://www.stsci.edu/ftp/science/hdf/hdf.html>). In addition to original images, this site provides a detailed description of observations, their processing, and calibration. It turned out that in the HDF-N, one can detect galaxies as faint as $B \sim 29^m$. Depending on the selection criteria, up to 2000–3000 galaxies in this field can be discovered (for comparison, only several dozen stars of our Galaxy were found). The main feature of the HST deep field is, of course, a much better resolution ($\approx 0."$ 1) than can be achieved by ground-based observations. Such an angular resolution enables one to study the observed structure of distant ($z \geq 1$) galaxies with the linear resolution ≤ 1 kpc. The principal shortcoming of the field is its small angular size (at $z = 1$, it corresponds to only ≈ 2 Mpc in the comoving frame), and therefore the statistics of objects in the field are not representative.

The first reproductions of the HDF-N (see, e.g., Fig. 6) clearly demonstrated that the Universe looked differently

several billion years ago. Distant galaxies are much more asymmetric, and there are numerous interacting and irregular systems. The Hubble field provided very rich data enabling the exploration of the morphology and sizes of galaxies, deep galaxy counts, searches for extremely distant objects ($z \geq 5$), etc.

The obvious success of the HDF-N stimulated carrying out an analogous project in the southern hemisphere [53]. Observations of the southern area (located in the Tucanus constellation) were carried out in October 1998. The HDF-S project has two important differences from the HDF-N: a remote quasar with $z = 2.24$ falls within this field and several instruments are simultaneously used. The following results were obtained: (1) a deep image of the field was obtained with the WFPC-2 (with the same filters and using the same methods as in the HDF-N), (2) the spectroscopy of the quasar in the spectral range 1150 to 3560 Å was made, an ultradeep image of a small area near the quasar was taken with the STIS (Space Telescope Imaging Spectrograph), and (3) a small area was imaged with the NICMOS (Near Infrared Camera and Multi-Object Spectrometer) at 1.1 μm, 1.6 μm, and 2.2 μm. All three instruments have different fields of view, and therefore the instrumental field must be specified in referencing the HDF-S. As in the case of the HDF-N, completely reduced observations of this field were open to access at the end of November 1998 (see <http://www.stsci.edu/ftp/science/hdfs.html>).

The policy of providing open access to the data, as well as their uniqueness (both fields had been the deepest ‘punctures’ into the Universe in several years), ensured that they were enormously popular and in demand. Both HDF areas were observed many times from the ground and from space and in all other spectral ranges, from X-ray to radio. According to ADS, at the beginning of 2005, the data of these fields were used in at least fifteen hundred papers.

4.3. CDF

The Chandra Deep Fields represent a series of deep (exposure ~ 10 –20 days) images of small patches of the sky obtained by the space Chandra X-ray Observatory (CXO). The best known of them are the North field (CDF-N) and South field (CDF-S). Observations of the CDF-S in the constellation Fornax were carried out in 1999–2000. The total exposure time was around 10^6 s. The CDF-S covered 0.109 sq. deg. with the pixel size 1". In the Southern Chandra field, 346 sources were discovered in the energy range 0.5–7 keV [54, 55]. Most of these sources are extragalactic objects, mainly active galactic nuclei and star-forming galaxies.

The CDF-N was the deepest X-ray image of the sky area obtained by the beginning of 2005. The field covers 0.124 sq. deg. with the total exposure time approaching $2 \cdot 10^6$ s. The coordinates of the Northern Chandra field are close to those of the HDF-N (see Section 2.4), but the

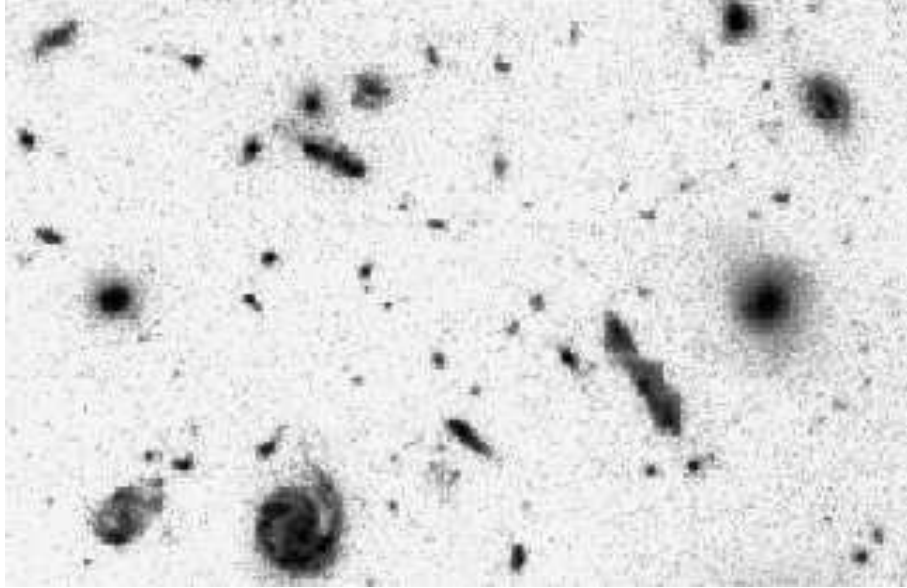


Fig. 6. A fragment ($\sim 20'' \times 30''$) of the HDF-N.

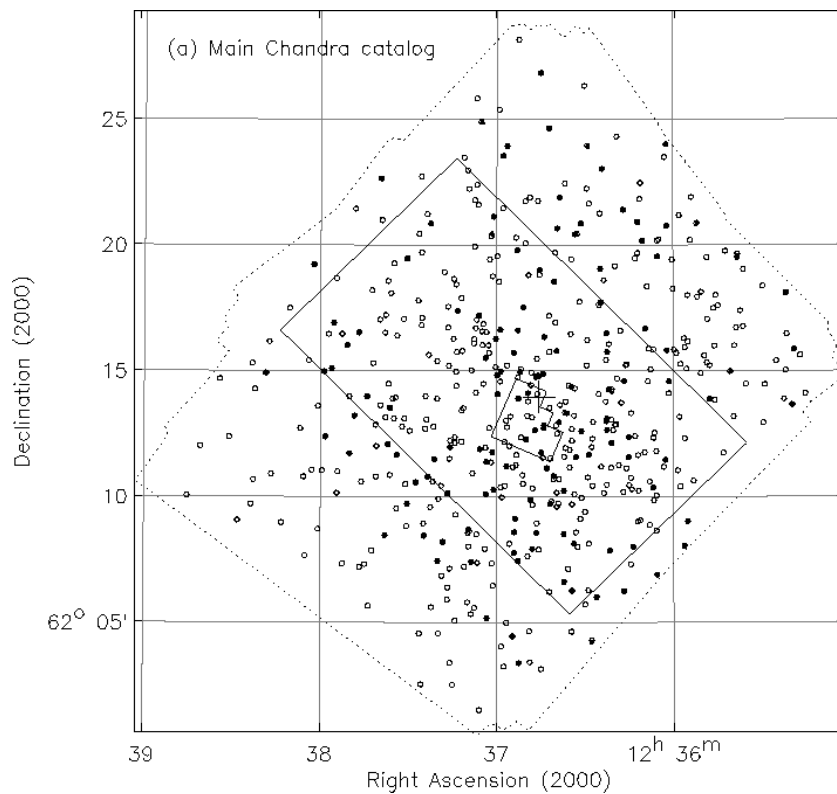


Fig. 7. The distribution of X-ray sources within the CDF-N (the boundaries of this field are shown by the dotted line). The white circles show sources detected with a 10^6 s exposure, the black circles stand for fainter sources that appeared when increasing the exposure time to 2×10^6 s. The small polygon in the center marks the HDF-N field.

area of the CDF-N is many times larger than HDF-N (Fig. 7). In the CDF-N, about 600 X-ray sources in the energy range 0.5–8 keV were discovered [56, 57]. Twenty of these sources lie within the HDF-N (Fig. 7).

Spectroscopic studies of optical counterparts of the CDF-S and CDF-N X-ray sources revealed that they lie at $z \sim 1$, with some sources having $z > 3$ (see, e.g., [57]).

For the first time, the CDF data enabled evaluating the evolution of the X-ray luminosity of active galactic nuclei as a function of z and investigating X-ray properties of normal galaxies at large redshifts [58].

4.4. FDF

The FORS Deep Field is devoted to a detailed photometric and spectroscopic study of a $\sim 7' \times 7'$ area located in the vicinity of the south galactic pole with the FOcal Reducer/low dispersion Spectrograph (FORS) on the 8.2-m ESO VLT telescope [59]. The main photometric observations were carried out in 1999–2000 with the UT1 (Antu) ESO VLT telescope with five broadband filters spanning the spectral range from ~ 3700 to ~ 8000 Å. With each filter, several dozen images were taken, and more than a hundred were obtained with the *R* filter. The total exposure time varied from 6 to 12 h depending on the color band. The image quality in the integral image is better than $1''$ in each filter. Near-IR observations (*J* and *K* filters) of the field were also carried out by the ESO NTT telescope.

A careful analysis of the FDF images allowed discovering almost 10,000 objects, mostly galaxies (only 50 stars are seen in the field). The limiting magnitude in the FORS field with filter *B* turns out to be comparable with that in the HDF (see Section 4.2), and is smaller than the HDF only by $\sim 1^m$ with the other filters. The ESO NTT telescope has started a spectral survey of the FDF objects. By the present time, redshifts for several hundred galaxies from this field have been reported (see e.g., [60]).

Additional observations of the FDF and data analysis continue. Some preliminary results on the physical properties of distant ($z > 3$) galaxies, their luminosity function evolution, the history of star formation in the Universe, etc., are reported in [61].

4.5. SDF and SXDS

The main goal of the Japanese project Subaru Deep Field (SDF) is to select and study a large sample of distant ($z > 4$) galaxies. Since 1999, the Japanese Subaru (Pleiades) telescope has been carrying out multicolor photometric and spectral observations of a $34' \times 27'$ area near the north galactic pole. Photometric data were obtained in five broadband (*B*, *V*, *R*, *i'*) and two narrowband filters in the near-IR wavelength range centered on 8150 Å and 9196 Å [62]. The central $2' \times 2'$ part of the SDF was also observed in *J* and *K* bands [63]. The total exposure time in each band was approximately 10 h with the limiting magnitudes near $28.^m5$ in the *B* filter and $23.^m5$ in *K*. More than 150,000 objects (mostly galaxies) were discovered in the Subaru Deep Field. The processed SDF images and catalogs of objects are available through <http://soaps.naoj.org/sdf/>.

Many interesting results on the properties and distribution of distant galaxies were obtained using the SDF. In particular, several objects with $z \geq 6$ were discovered (their age is only several million years), including the most distant, at the present time, spectroscopically confirmed $\text{Ly}\alpha$ -emitting object with $z = 6.60$ [64].

The Subaru/XMM-Newton Deep Survey (SXDS) is a multi-wavelength survey of a small (~ 1.3 sq. deg.) area

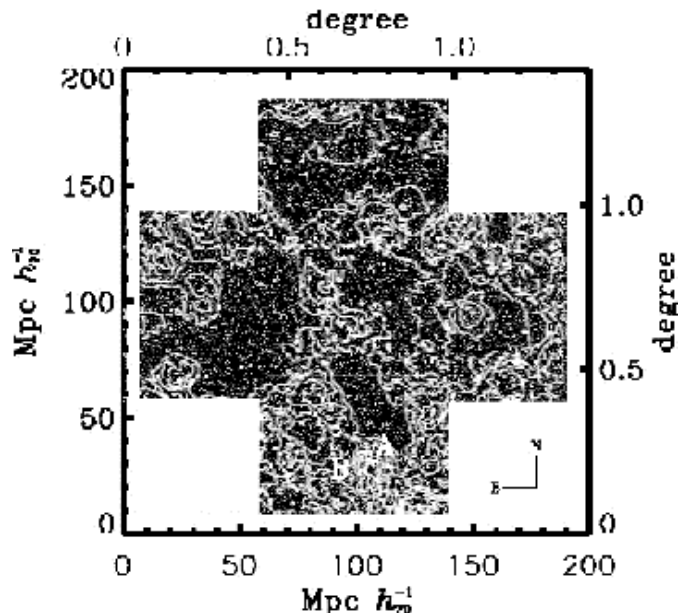


Fig. 8. The distribution of $\text{Ly}\alpha$ -emitting objects with $z = 5.7 \pm 0.05$ in the SXDS (the light contour lines).

obtained with several ground-based and space instruments (Subaru, UKIRT, XMM-Newton, VLA, GALEX, JCMT) (see, e.g., [65]). The SXDS is centered at $\alpha(2000) = 2^h 18^m 00^s$ $\delta(2000) = -5^\circ 00' 00''$. This survey is less deep (in terms of the limiting magnitude) than the SDF, but has a coverage several times larger and, in addition, allows multi-wavelength studies of objects.

At the end of 2003, photometric observations of the SXDS field were performed in a narrow band centered on $\lambda = 8150$ Å. Using a special method based on comparison of the energy flux density in different spectral intervals, more than 500 candidates in galaxies with $z = 5.7 \pm 0.05$ were selected [66]. Spectral observations confirmed that most objects must actually reside at such z . From analysis of the space distribution of galaxies, the authors of [66] arrived at the conclusion that some primordial large-scale structure of galaxies with extended filaments, voids, and even with two clusters under formation (see Fig. 8) must already exist at $z = 5.7$ (!).

4.6. COMBO-17

COMBO-17 (Classifying Objects by Medium-Band Observations in 17 filters) represents a multicolor photometric survey of five $\sim 0.95 \times 0.95$ areas (including the CDF-S, the south galactic pole, and the Abell 901/902 supercluster) obtained with the 2.2-m MPG/ESO telescope in Chile [67,68]. The main feature of this project is that observations were carried out with 17 filters (five broadband – *U*, *B*, *V*, *R*, *I*, and 12 medium-band) covering the spectral range 3500–9300 Å. Such a detailed photometry allows constructing a kind of low-resolution spectrum of each object, which can be used both to spectrally classify and to evaluate the redshift of each object with a relatively

good accuracy ($\sigma_z \approx 0.03$). The relatively small depth of COMBO-17 ($B \approx 25.5$ [68]), therefore, is compensated by the large coverage, as well as by the possibility of estimating the type and z of an object without additional spectral observations. These advantages of COMBO-17 make it a convenient tool to study galaxies using the weak gravitational lensing method [69].

The results obtained in this project for the Southern Chandra Field, including a catalog of 63,501 objects, were recently published in [70] (see also http://www.mpia.de/COMBO/combo_index.html).

4.7. GOODS

In January 2004, a special issue of the *Astrophysical Journal Letters* was entirely devoted to preliminary results obtained in the GOODS (Great Observatories Origins Deep Survey) project [71]. The GOODS is a new-generation project after the HDF, combining deep multi-wavelength observations from several space (HDF, SIRTf, CXO, XMM-Newton) and ground-based (ESO VLT, ESO NTT, KPNO 4-m, etc.) telescopes. The scientific goals of the GOODS include estimations of stellar and dynamical masses of bright galaxies up to $z \sim 5$, measurements of the star formation rate in complete samples at different z , studies of the origin of the Hubble sequence, measurements of the relative contributions of stars and active galactic nuclei to the global energy budget of the Universe, and studies of individual sources contributing to intergalactic background radiation in all spectral ranges.

Observations have been carried out in two areas ~ 160 sq. min., each almost centered on the HDF-N (Section 4.2) and CDF-S (Section 4.3).

The fields were observed with the HST by the Advanced Camera for Surveys (ACS) installed in 2002 in four broad-band filters F435W (B), F606W (V), F775W (i), and F850LP (z) (the three figures in the filter's name indicate the central wavelength in nm). As with the HDFs, dozens of dithered exposures are taken with each filter. Observations in V , i , and z were carried out during five periods delayed by 40–50 days. (Such an observational strategy was adopted to facilitate searches for distant ‘cosmological’ supernovae. As a result, more than 40 supernovae were discovered by the GOODS, with six SN Ia’s at $z > 1.25$ [72].)

After initial reductions and the superposition of individual frames, integral images of the fields in all filters were obtained with the step $0.''03$ (the actual angular resolution in the images is $\approx 0.''1$). The limiting magnitude of extended objects in these fields is by $0.^m5$ – $0.^m8$ worse than in the previous HST deep fields, but the total coverage of the GOODS is 30 times larger than that of the HDF-N and HDF-S taken together. The original HST frames and reduced images are available through the web pages of the GOODS project: <http://www.stsci.edu/science/goods/>.

Observations in the framework of the GOODS project with other telescopes (including, in particular, Keck and

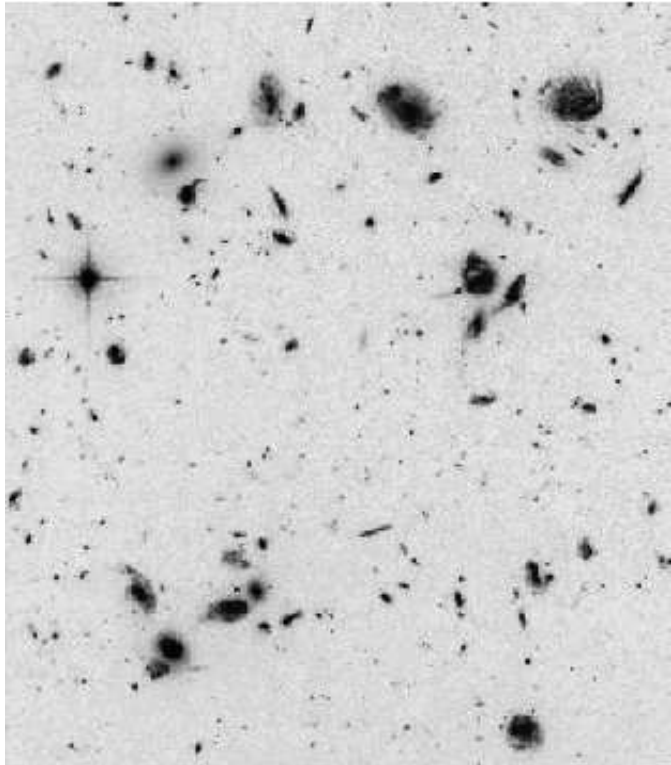


Fig. 9. Detail $\sim 50'' \times 55''$ of the HUDF.

Gemini) either have already been made or are being carried out. See paper [71] or the project web page for details.

4.8. HUDF

The Hubble Ultra Deep Field (HUDF) is the deepest optical imaging of a patch of the sky ever made (Fig. 9). The authors of the project believe it will remain such in the next several years and, consequently, this field will long remain the main source of information on the most distant objects in the Universe [73].

The HUDF is located within the limits of the Southern Chandra Field (CDF-S) and, hence, within the GOODS field. The precise coordinates of the HUDF are $\alpha(2000) = 3^h 32^m 39^s.0$ and $\delta(2000) = -27^\circ 47' 29.''1$. Major observations were carried out by the HST from September 2003 till January 2004 with a wide-field camera (WFC) ACS with the same four filters as the GOODS observations. The field coverage is relatively small: 11.5 sq. min. More than a hundred individual images were taken in the B and V filters with the total exposure time $\sim 40^h$. Observations in the i and z bands include almost 300 frames with the total exposure time $\sim 100^h$ with each filter.

The final calibrated HUDF images with the step $0.''03$ (the image size with each filter is 430 Mb) and the catalog of discovered objects can be found on the web page of the project: <http://www.stsci.edu/hst/udf>. The HUDF is by about one magnitude deeper than the HDF. In this field, around 10,000 galaxies up to $B \sim 30^m$ ($\sim 5 \cdot 10^{-9}$ Jy!) were discovered.

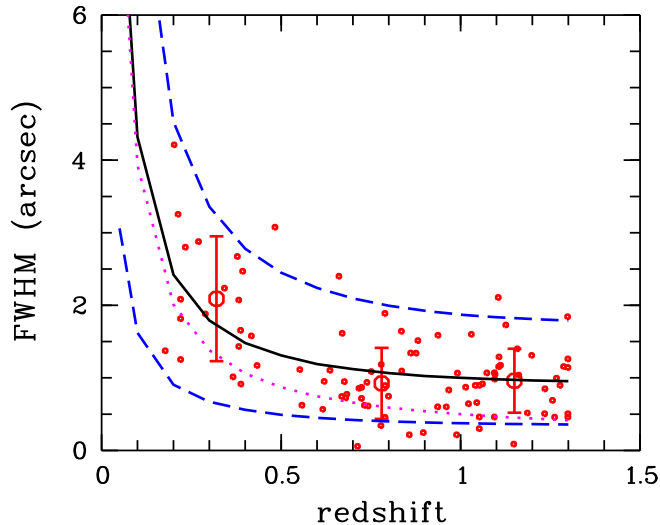


Fig. 10. The angular size of bright galaxies as a function of z (red points). The circles with bars show the mean values and corresponding dispersions for three intervals of z . The dashed lines are the lines of constant linear sizes (the bottom and upper lines correspond to the respective linear sizes 3 kpc and 15 kpc). The solid line shows the dependence of the linear size on z for a galaxy with FWHM=8 kpc (FWHM is the full width at the half-maximum brightness). The dotted line shows the expected change in the angular size of a galaxy according to the law $\propto (1+z)^{-1}$ as predicted by some models.

To improve the impact of the ACS data, the central part of the HUDF was also observed by the HST with the NICMOS (Near-Infrared Camera and Multi-Object Spectrometer) with filters F110W (J) and F160W (H). An unprecedented depth was also attained in these observations: the limiting apparent magnitudes in the J and H bands are $\approx 27.^m5$ ($\sim 1.5 \cdot 10^{-8}$ Jy) [74]. Such high-quality data in the near-IR spectral range make the HUDF an extremely valuable field for selecting and studying the most distant objects. The first analysis of the HUDF allowed discovering galaxy candidates at $z \sim 7-8$ (see, e.g., [74]).

In parallel with the main observations, the HUDF field has been studied with other HST instruments: the STIS (Space Telescope Imaging Spectrograph) and the WFPC-2 (Wide-Field Planetary Camera 2). These observations and results are summarized on the STScI site: <http://www.stsci.edu/hst/udf>.

4.9. Other projects

Above, we have briefly described typical or unique projects. This list of notable deep field projects is far from being complete, but it is impossible to describe all of them. For completeness, below I briefly enumerate several other interesting projects.

The LCRS (Las Campanas Redshift Survey) is a spectroscopic survey of ~ 2600 galaxies with the 2.5-m tele-

scope of the Las Campanas observatory (Chile) [75]. The survey covers about 700 sq. deg. and consists of six extended patches $1.^{\circ}5 \times 80^{\circ}$ each.

The NDF (NTT Deep Field) represents a deep ($B \leq 27.^m5$) photometry of a small (~ 5 sq. min.) area with the 3.6-m ESO NTT telescope [76].

The CNOC2 (Canadian Network for Observational Cosmology) is a survey covering ~ 1.5 sq. deg. of the sky with the 3.6-m CFHT telescope [77]. The survey is aimed at determining redshifts for ~ 6000 galaxies with the apparent magnitude $R \leq 21.^m5$ and providing multicolor photometry for $\sim 40,000$ galaxies with $R \leq 23.^m$.

The MUNICS (Munich Near-Infrared Cluster Survey) represents a photometric and spectroscopic study of several thousand galaxies with $K \leq 19.^m5$ within several areas with the total coverage ~ 1 sq. deg. [78] The photometry was obtained with the 2.2-m and 3.5-m telescopes of the Calar Alto observatory (Spain). The Hobby-Eberly (9.2-m, USA) and ESO-VLT telescopes were also used for spectral observations.

K20 is a spectroscopic survey of a complete sample of galaxies with the apparent magnitude $K < 20.^m$ (around 550 objects) within two fields covering ~ 52 sq. min. with the ESO VLT telescope [79].

The DEEP2 (Deep Extragalactic Evolutionary Probe 2) is a spectroscopic survey covering ~ 3.5 sq. deg. of the sky with a multi-object spectrograph on the 10-m Keck-II telescope [80]. Redshifts for $\sim 60,000$ remote ($z > 0.7$) galaxies will be measured.

GEMS (Galaxy Evolution from Morphologies and SEDs) represents the largest ($\sim 28' \times 28'$) image obtained up to the present time with the Hubble Space Telescope [81]. The field was observed with two filters (F606W and F850LP). The integrated image represents a mosaic from about 60 WFC ACS fields. The GEMS field is centered on the CDF-S and includes the GOODS field. The size and location of GEMS are almost identical to the COMBO-17. The GEMS data allow the study of the structure and morphology of $\sim 10,000$ galaxies.

The VVDS (VIMOS-VLT Deep Survey) is a photometric and spectroscopic survey of $\sim 100,000$ galaxies within several deep fields covering ~ 16 sq. deg. with the VISIBLE Multi-Object Spectrograph (VIMOS) on the ESO VLT telescope [82, 83].

The OACDF (Capodimonte Deep Field) is a multi-color (9 color bands) photometric survey of $\sim 50,000$ galaxies within a ~ 0.5 sq. deg. field with the ESO/MPG 2.2-m telescope [84].

The NDWFS (NOAO Deep Wide-Field Survey) is a deep optical and near-infrared imaging survey covering two 9.3 sq. deg. fields with the KPNO and CTIO telescopes (<http://www.noao.edu/noao/noaodeep/>).

COSMOS is an HST Treasury project to perform a survey using the ACS in a single filter (F814W) in a contiguous 2 sq. deg. equatorial field (<http://cosmos.astro.caltech.edu>). The selection of an equatorial field has allowed observatories in both hemi-

spheres to join efforts for the extensive follow-up multi-wavelength observations.

This list is of course incomplete. In particular, there are many purely spectroscopic galaxy surveys in small fields, which are referenced in papers cited above.

The description of the projects shows that virtually all the largest ground-based telescopes are participating in deep field studies and surveys. The largest Russian 6-m telescope of SAO RAN (BTA) is no exception. Shortly after its construction (1976), deep galaxy counts near the north galactic pole were carried out with this instrument [85]. These counts (the black box in Fig. 2 a,b) were followed up to $B \approx 26^m$, which was one of the best results at that time.

The possibilities of the BTA are well illustrated by paper [86] reporting the results of four-color photometry of a small ($3.6 \times 3'$) field centered at the gamma-ray burst GRB 000926. Around 300 objects with $B \leq 26.6^m$ were found in this field (the black circle in Figs 2 a,b). Both differential galaxy counts and their general characteristics turned out to be in agreement with the results of other deep fields. An analysis of images of bright ($M(B) < -18^m$, where $M(B)$ is the absolute magnitude in filter B) spiral galaxies led to the conclusion that there is no strong evolution of their linear sizes at $z \leq 1$ (Fig. 10, [86]).

5. Some results

In this Section, we briefly report selected results of the described projects. We describe very general *observational* results on the mean characteristics of galaxies.

5.1. Galaxy counts

Over many years, galaxy counts, i.e., the plot of the observed number of galaxies at the limiting magnitude, have been considered to be an important cosmological test. In particular, in the 1930s, Hubble tried to apply them to estimate the curvature of space. It became clear later that practical application of this test is so difficult (photometric errors, the account for k -correction, the evolution of galaxies with time) that “any attempt to do so appears to be a waste of telescope time” [87]. Presently, deep counts are regarded not as a cosmological test but rather as a test of galaxy formation and evolution.

Figure 11 summarizes modern results of differential galaxy counts according to data from the web page <http://star-www.dur.ac.uk/~nm/pubhtml/counts/counts.html>. Only data obtained after 1995 are shown. With each filter, the results of about twenty projects (including 2MASS, SDSS, HDF, CDF, NDF, etc.) are summarized; with filter B , counts in the SDF, VVDS, and HUDF fields are added. The figure shows good agreement between the results of different works. For example, for $B \approx 25^m$, the count dispersion is only about 10% (accounting for the photometry, different selection of galaxies, etc., this dispersion must be even smaller), which clearly

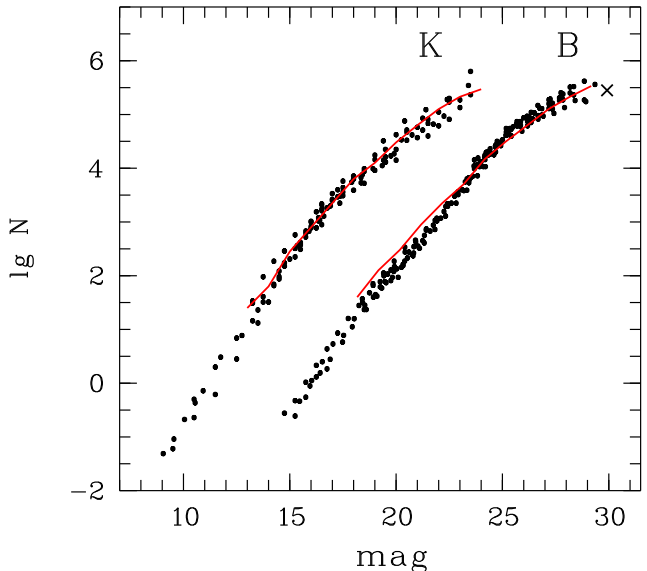


Fig. 11. Differential counts of galaxies (the number of galaxies within a given range of apparent magnitudes normalized to 1 square degree) with filters B and K (dots). Data in filters B and K are calculated using 0.5^m and 1.0^m intervals, respectively. The cross marks the HUDF galaxy counts. The solid lines show predictions of the galaxy formation model in [88].

illustrates the homogeneity and isotropy of large-scale galaxy distribution. For brighter (and, on average, closer) objects, the count dispersion increases due to large-scale structure effects. The weakest source counts strongly suffer from photometric errors and other factors.

The solid lines in Fig. 11 show predictions of a semi-analytic model of galaxy formation [88] (the ‘LC’ model in that paper). Both this and other models (see, e.g., [89] and the references therein) can satisfactorily fit observations. However, the model predictions are not fully definitive due to many parameters characterizing galactic properties and their evolution with z (including spatial density evolution). For further progress in this field, both observational data and theoretical understanding of galaxy evolution must be improved.

5.2. Galaxy distribution

The distribution of galaxies in the nearby volume of the Universe is highly inhomogeneous (Figs 3, 4). When passing to the hundred Megaparsec scale, the density fluctuations smoothen and the distribution becomes more homogeneous (Fig. 5).

The clustering of galaxies is usually described in terms of two-point correlation functions $\xi(r)$ and $\omega(\theta)$. The former function describes the joint probability of finding two galaxies separated by a distance r , and the latter characterizes the joint probability of detecting two objects at the angular distance θ [90]. To calculate $\xi(r)$, spatial distances between galaxies should be known, and in practice it is

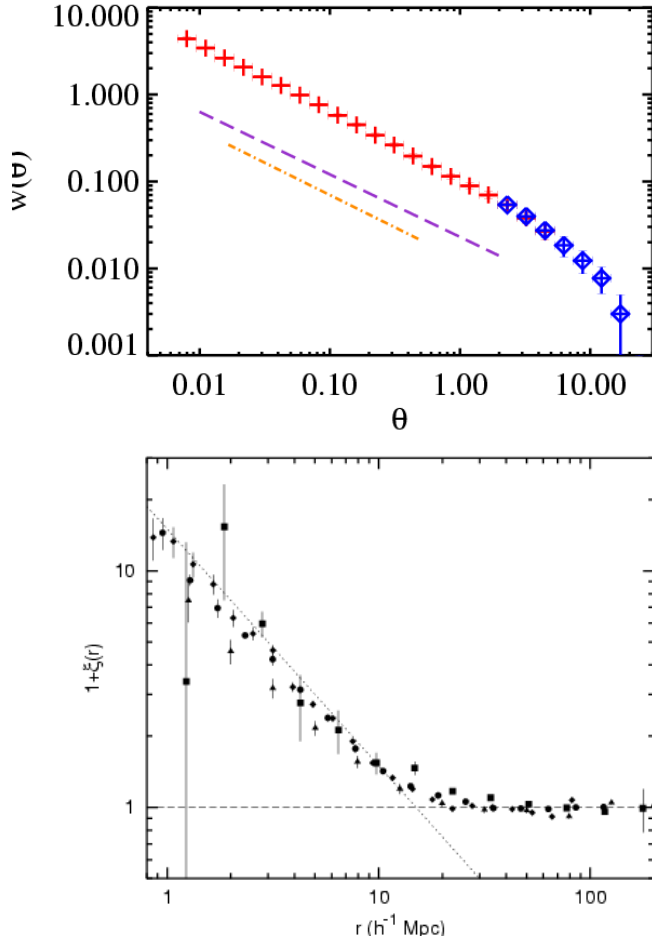


Fig. 12. Top: the two-point angular correlation function $\omega(\theta)$ (the angle θ in the plot is measured in degrees) for 2MASS galaxies (crosses and diamonds). The dashed and dot-dashed straight lines plot linear approximations of the data obtained in the APM and SDSS surveys, respectively [91]. Bottom: the two-point correlation function $\xi(r)$ according to data from different surveys (including APM, LCRS, etc.) [92].

Fig. 13. Density fluctuations $\delta\rho/\rho$ as a function of scale [94] The solid line marked with CDM shows the prediction of a flat CDM model (the model with ‘cold dark matter’). The ‘hot dark matter’ model prediction is marked with HDM.

therefore more convenient to measure the (angular) two-point correlation function $\omega(\theta)$. From $\omega(\theta)$, one can then estimate $\xi(r)$ because both functions are related through the Limber integral equation. If $\xi(r)$ can be represented as a power law $\xi(r) = (r/r_0)^{-\gamma}$, the angular correlation also takes a power-law form $\omega(\theta) \propto \theta^{1-\gamma}$ [90].

Figure 12 plots the angular correlation function for ~ 0.5 million galaxies from the 2MASS survey [91]. At angular scales $1' < \theta < 2.05'$, this function is well fit by a power law with $1 - \gamma = -0.79 \pm 0.02$. The amplitude of $\omega(\theta)$

depends on the sample depth – for brighter and closer objects, the clustering amplitude increases (this, in particular, explains the systematic shift between different survey data in Fig. 12).

In the bottom part of Fig. 12, we show the correlation function $\xi(r)$ calculated in different papers (h in the figure means the Hubble constant value expressed in units of 100 km/s/Mpc). In the range $0.1 \text{ Mpc} \leq r \leq 20 \text{ Mpc}$, this function follows a power law with the exponent $\gamma \approx 1.7 - 1.8$, and then tends to zero. The characteristic clustering scale (correlation length) r_0 for nearby galaxies is $\approx 7 \text{ Mpc}$. The correlation length depends on the properties of galaxies, such as their luminosity and morphological type (see, e.g., [93]), but is independent of the sample depth (see the discussion in [92]).

Modern survey data allow determining the density fluctuations in the Universe as a function of the scale of averaging (Fig. 13). (The power spectrum of the SDSS galaxies, which has been used to plot this figure, is based on data on $2 \cdot 10^5$ galaxies [95].) Figure 13 shows that different kinds of data, from galaxy density fluctuations to cosmic microwave background anisotropy, form a unique smooth dependence described by the CDM model.

Recently completed surveys have allowed features of the nearby galaxy distribution to be studied in a detail unavailable earlier. In particular, the 2MASS survey enabled examining the galaxy distribution in the ‘zone of avoidance’ the strip near the Milky Way plane ($|b| < 10^\circ$) where the interstellar absorption screens extragalactic objects [96]. The galaxy distribution as derived from the 2MASS, 2dF, and APM surveys led to the conclusion that there is a 30% deficit of bright galaxies in the southern galactic hemisphere in comparison with the northern one [97]. The authors believe that the observed deficit is a consequence of a huge ‘hole’ with a linear size possibly exceeding 200 Mpc in the local galaxy distribution. Such a large local nonhomogeneity, as well as the possible presence of a well-defined large-scale structure at $z \sim 6$ ([66], see Section 4.5; [98]), can pose certain problems for the standard CDM model. We note that nonhomogeneities of a comparable scale ($\geq 200 \text{ Mpc}$) have been found in the quasar distribution derived from the 2QZ project (see Section 3.5) [99].

5.3. Evolution of the luminosity function

The luminosity function (LF) is the dependence of the number of galaxies within a unit volume on their luminosity. It is one of the most important integral characteristics of galaxies. The LF allows estimating the mean luminosity density in the Universe. The LF form is one of the main tests of galaxy formation models. The standard form of the LF is the so-called Schechter function [100]

$$\phi(L)dL = \phi_* \left(\frac{L}{L_*}\right)^\alpha \exp\left(-\frac{L}{L_*}\right) d\left(\frac{L}{L_*}\right),$$

where $\phi(L)dL$ is the number of galaxies with the luminosity from L to $L + dL$ per unit volume, and ϕ_* , L_* and α are parameters. The parameter ϕ_* yields the normaliza-

tion of the LF, L_* is the characteristic luminosity, and α determines the slope of the weak wing ($L < L_*$) of the LF: the weak wing of the LF is flat for $\alpha = -1$, the LF increases with decreasing L for $\alpha < -1$, and decreases at $\alpha > -1$. The Schechter function fits well the real LF of field galaxies and clusters and has convenient analytical properties.

At present, the local LF of galaxies is relatively well studied. According to many papers (including the 2dF and SDSS surveys), within the absolute magnitude range $-15^m \geq M(B) \geq -22^m$ (filter B), the LF can be described with the following values of parameters:

$$\alpha \approx -(1.1 - 1.2),$$

$$M_*(B) \approx -20.^m2 \quad (L_*(B) = 1.9 \cdot 10^{10} L_{\odot,B}), \text{ and}$$

$$\phi_* \approx (0.5 - 0.7) \cdot 10^{-2} \text{ Mpc}^{-3} \text{ (see. e.g., [101]).}$$

Therefore, the luminosity density of galaxies at $z = 0$ is

$$\rho_L(B) = \phi_* L_* \Gamma(\alpha + 2) \approx 1.3 \cdot 10^8 L_{\odot,B} / \text{Mpc}^3$$

and the galaxy density is

$$\rho = \rho_L / L_* = \phi_* \Gamma(\alpha + 2) \sim 10^{-2} \text{ Mpc}^{-3}.$$

The LF of local galaxies depends on their morphological type and environment [102].

Numerous deep field studies performed over the last ten years have enabled the evolution of the LF with z to be determined. In solving this problem, the so-called ‘photometric redshifts’ inferred from multicolor photometry are used instead of spectroscopic ones for the most distant objects. Such a photometry allows a kind of a low-resolution spectrum and hence z of an object to be obtained. Photometric estimations of z are being made with $\approx 10\%$ – 20% accuracy, which is quite sufficient to derive the LF for large samples of galaxies.

Observations suggest a differential (depending on the galaxy type and the color band) evolution of the LF. Different papers give somewhat different results, but the qualitative picture emerging is as follows: the value of M_* increases with z , while ϕ_* decreases (Fig. 14). According to [103], towards $z \sim 5$, the value of M_* in filter B increases by 1^m – 2^m , and ϕ_* decreases by 5–10 times. The evolution of the LF slope is much less definitive, although some authors note a decrease in α with z . By considering different types of objects separately, the space density of elliptical and early spiral galaxies almost stays constant or slightly decreases toward $z \sim 1$, while their LF evolution can be described as a change in the luminosity of galaxies (they become brighter). In contrast, the space density of late spiral galaxies with active star formations notably increases toward $z \sim 1$ [104, 105]. The change in the LF of galaxies alters the luminosity density they produce: from $z = 0$ to $z \sim 3$, the value of ρ_L increases, with the strongest growth being in the UV region (by about 5 times [106]).

5.4. Evolution of the galaxy structure

One of the main goals of the deep field galaxy studies is the origin and evolution of the Hubble sequence. In the local Universe, the optical morphology of the vast majority

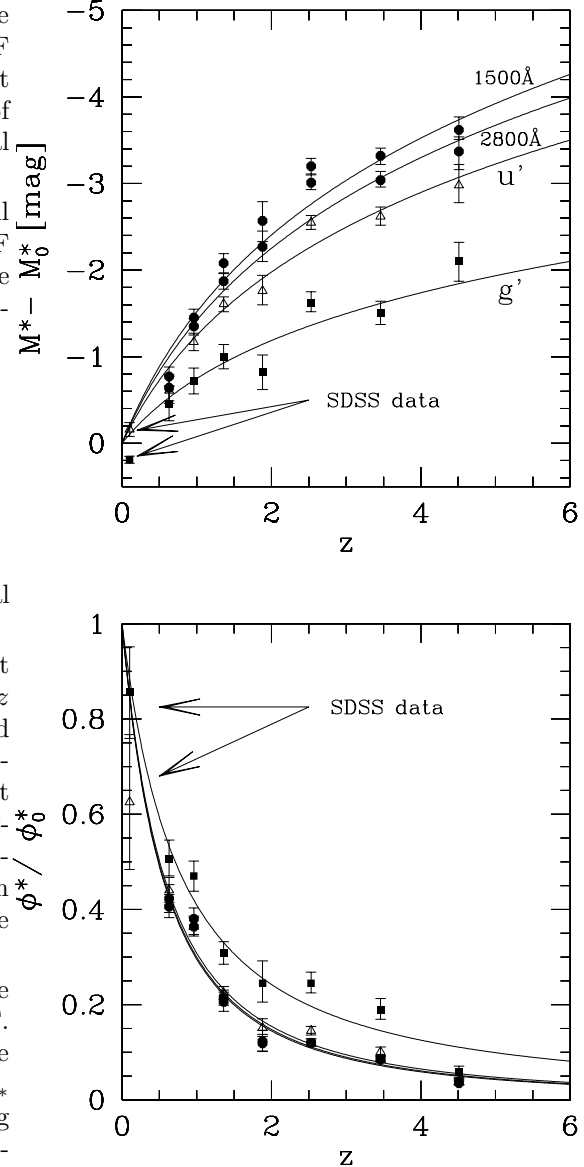


Fig. 14. The redshift dependence of the parameters of the luminosity function of galaxies M_* (top) and ϕ_* (bottom) [103]. Different color bands are marked with different signs. The solid lines show analytic approximations of the observational data. The LF parameters as derived from the SDSS survey are shown by arrows.

of bright galaxies can be described in terms of a simple classification scheme suggested by Hubble [3]. Only about 5% of nearby objects do not fit this scheme and are related to irregular or interacting galaxies [107, 108].

The deep HST fields for the first time allowed us to see the structure of distant galaxies. The very first studies revealed that the fraction of galaxies that do not fit the Hubble scheme increases for fainter objects [109]. At $z \sim 1$ (where the age of the Universe is about half the Hubble time), the fraction of such galaxies reaches 30%–40% (see examples in Figs 6 and 9). The lack of a convenient clas-

sification for distant galaxies stimulated the development of new methods for analyzing their images and the construction of objective classification schemes invoking the characteristics such as asymmetry and concentration indices (see, e.g., [109, 110]).

The statistics of objects in some deep fields also suggests that the fraction of interacting galaxies and merging galaxies increases with z . With the $(1+z)^m$ growth assumed, observational data suggest $m \approx 2-4$ for $z \sim 1$ [111, 112]. The evolution of the merging rate is likely to depend on the mass of galaxies – it is most pronounced for massive objects [112].

It is much more difficult to draw definitive conclusions on the structure evolution for objects at $z \geq 1$ due to the increasing effects of the k -correction, the cosmological dimming of surface brightness and degradation of the resolution [113]. The history with bar studies for distant galaxies may serve as an instructive illustration. The first morphological studies of galaxies in the HDF implied a drastic decrease in the fraction of barred spirals at $z > 0.5$, but the subsequent analysis indicated that this fraction remains almost constant ($\sim 40\%$), at least up to $z = 1.1$ [114, 115].

A significant amount of observational data has been obtained about changes in the characteristics of large-scale subsystems of galaxies. For example, it has been established that by $z \sim 1$, the disk surface brightness of spiral galaxies increases by $\sim 1^m$, while the color indices decrease (i.e., become ‘bluer’) [116, 117]. For $z \leq 1$, a change in the slope of the Tully–Fisher relation is found (the Tully–Fisher relation is the dependence between the maximum rotation velocity and the luminosity of spiral galaxies) [118]. This slope change is believed to be a consequence of the differential evolution of spiral galaxies: at $z \sim 1$, low-mass spirals become brighter by 1^{m-2m} , while massive ones stay virtually as bright. Disks of ‘edge-on’ spirals at $z \sim 1$ show a larger relative thickness (the ratio of the vertical and radial scales in the brightness distribution) and demonstrate vertical deformations of the plane (warps) more frequently than nearby objects [119, 120]. Spectral studies of spiral galaxies suggest their chemical composition evolution: from $z = 0$ to $z = 1$, the metallicity of gas subsystems of galaxies decreases [121].

Some papers have investigated photometric and kinematical characteristics of elliptical galaxies in the field and in clusters up to $z \sim 1$ (see, e.g., [122, 123]). A deviation of distant early-type galaxies from the Fundamental Plane determined by the nearby objects has been discovered. This deviation is explained by the so-called ‘passive’ evolution of their luminosities and, correspondingly, the mass–luminosity ratio (see [40, 124] for more details).

5.5. The most distant galaxies

Searches for and studies of the most distant galaxies in the Universe are some of the most interesting and important fields of extragalactic astronomy. The most distant and hence the youngest galaxies provide invaluable tests

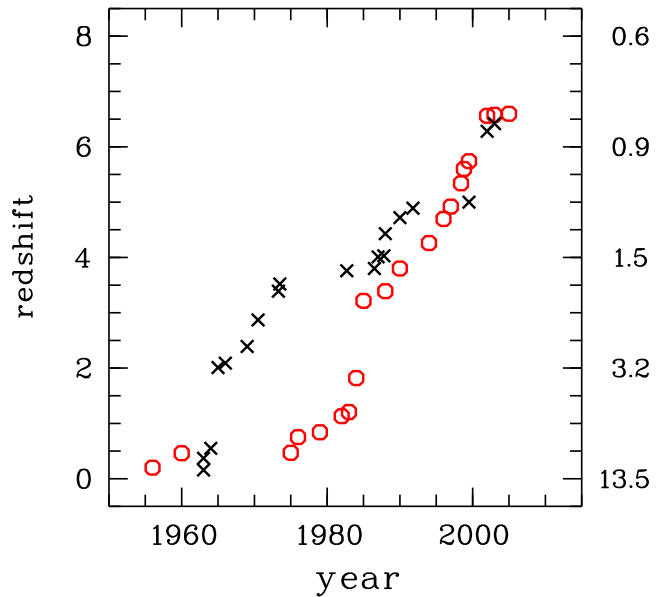


Fig. 15. The history of detection of the most distant objects in the Universe (the circles are for galaxies, the crosses are for quasars). Years when the objects were discovered are plotted along the horizontal axis. Along the vertical axis to the left are plotted redshifts, and to the right – time in billions of years since the beginning of the cosmological expansion. The plot relies on the data in review [125] added with data obtained in recent years.

of galaxy formation models and allow processes in the relatively early Universe to be studied.

The history of discoveries of the most distant galaxies is shown in Fig. 15. It is seen that quasars had been the most distant objects over almost three decades. (The term ‘quasar’ itself had often served as a synonym for the most distant objects.) The explanation is simple, because quasars are associated, as a rule, with very bright galaxies whose spectra show powerful and wide emission lines. The brightness of quasars and lines in their spectra make them much easier to observe from cosmological distances than ordinary galaxies (for example, see the spectrum of a distant quasar in Fig. 16). At the beginning of the new millennium, new methods appeared that allowed a very effective selection of ordinary galaxies at high z ; since then, these galaxies and not quasars have been the most distant known objects in the Universe (Fig. 15).

There are several methods of selecting galaxies at high z . Analysis of broad-band color indices to find galaxies with peculiar colors (see Section 2) is one of the most effective means of selecting very distant galaxies. This method is primarily aimed at searching for galaxies with an energy distribution break near the Lyman continuum (912 Å), which is expected in star-forming galaxies [9]. Due to the absorption in $L\alpha$ clouds along the line of sight, emissions in the spectra of distant galaxies between 912 Å and the $L\alpha$ line are absorbed. This creates an additional spectral feature that allows distant galaxies to be selected by

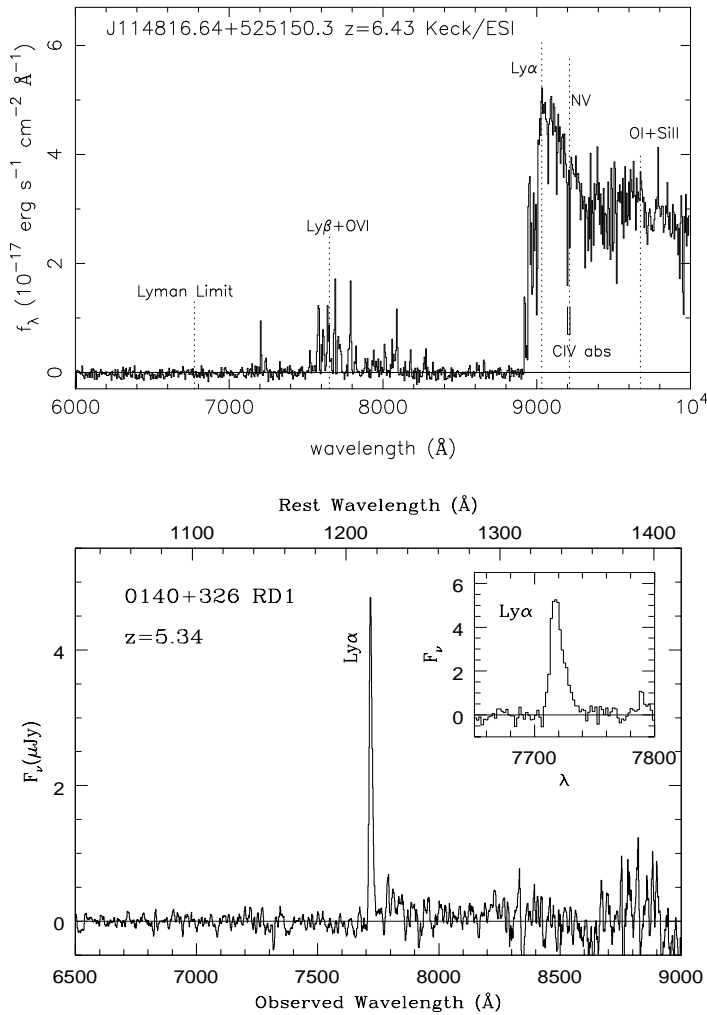


Fig. 16. The spectrum of a quasar with $z = 6.4$ (top) [126] and the spectrum of a galaxy with $z = 5.34$ (bottom) [127].

their broad-band color indices. More than a thousand objects with $z > 2.5$ have been selected using this method; they are commonly referred to as Lyman-break galaxies or simply LBGs (see [9] for a detailed review).

The second method frequently used is the search for galaxies showing a strong emission $L\alpha$ line using a deep narrow-band photometry of individual areas of the sky followed by a spectroscopic study of the detected objects (see Section 2 for more details). Objects found this way are often called ‘ $L\alpha$ emitters,’ or LAEs. It is by using this method that the most distant object known so far with $z = 6.60$ was discovered and signs of the presence of a large-scale structure of galaxies at $z = 5.7$ were found (Section 4.5).

At present, more than thirty galaxies with spectroscopic $z > 5$ have been reliably detected [64, 128] (see an example of the spectrum in Fig. 16). The age of such objects does not exceed $\sim 10\%$ of the age of the Universe (Fig. 15). Distant galaxies have been discovered both in

deep fields and near galaxy clusters enhancing fluxes from remote background galaxies due to gravitational lensing.

The main observational features of galaxies with $z > 5$ (see, e.g., [64, 129]) are as follows:

- as a rule, morphologically peculiar, asymmetric, compact shapes (the characteristic linear size is 1–5 kpc);
- a very high surface brightness and luminosity (corrected for the cosmological brightness decrease and k -correction effects);
- equivalent widths of the $L\alpha$ line in the comoving frame are $W(L\alpha) \sim 20\text{--}100 \text{ \AA}$;
- the star formation rate inferred from the $L\alpha$ line luminosity is $\sim 5\text{--}10 M_{\odot}/\text{yr}$ (this rate estimated from the UV continuum luminosity is several times larger).

These characteristics are very strongly biased by the selection procedure itself, and it is therefore unclear to what extent they reflect actual properties of all objects located at $z > 5$. The observed objects can be ‘building blocks’ that later merge and accrete the surrounding matter to form the galaxies we now know in our vicinity. On the other hand, some of these objects can represent bulges of massive spirals under formation or elliptical galaxies.

The clustering of LBGs and LAEs has been studied in some papers. For bright galaxies ($L \geq L_*$), the clustering scale r_0 does not show significant evolution from $z = 0$ to $z = 5$ [130, 131]. In contrast, the ‘bias parameter’ b characterizing the difference in space distribution of galaxies and dark halos increases several times toward $z = 5$ [131]. The GOODS and HUDF results may indicate an evolution in galaxy sizes: from $z \sim 2$ to $z \sim 6$, the mean linear sizes decrease by about two times [132, 133]. Both the galaxy clustering evolution and change in the galaxy sizes can be explained by the CDM model of galaxy formation.

The spectra of the most distant galaxies and quasars provide the possibility of studying an early evolution of the intergalactic medium. In particular, the so-called Gunn–Peterson effect [134] (a trough in the spectra of distant objects shorter than $L\alpha$ due to absorption by neutral hydrogen clouds along the line of sight) allows estimating the redshift at which the secondary ionization epoch (re-ionization) of the Universe has been completed [135]. The discovery of this effect in spectra of quasars with $z > 6$ (Fig. 16) and its absence for objects with $z \leq 6$ suggest the re-ionization epoch (i.e., ionization of the intergalactic medium by radiation from star formation regions and active galactic nuclei) to have been completed by $z \sim 6$ [136, 126]. On the other hand, the cosmic microwave background anisotropy measurements may evidence the beginning of secondary ionization at $z \sim 20$ (see, e.g., review [137]). The combination of these data has led to the conclusion of a complicated, possibly two-stage, history of the secondary ionization of the intergalactic medium [138].

5.6. History of star formation in the Universe

Reconstruction of the global history of star formation in the Universe from $z \sim 6$ until now appears to be one of

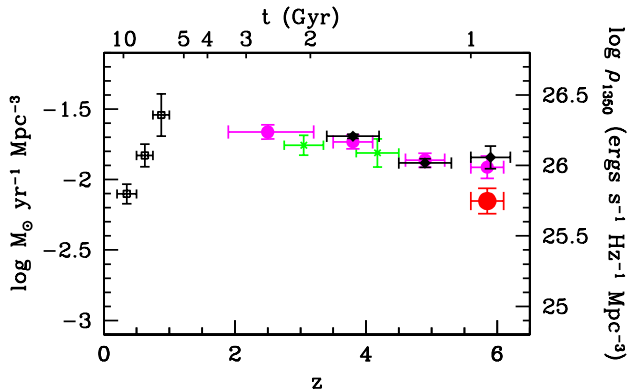


Fig. 17. The history of star formation in the Universe [140]. The specific star formation rate in units $M_{\odot}/\text{yr}/\text{Mpc}^3$ is plotted to the left, the luminosity density at $\lambda = 1350 \text{ \AA}$ is plotted to the right. The upper horizontal axis plots the time since the beginning of the cosmological expansion.

the most intriguing results derived in recent years from sky surveys and deep fields. Quantitative results by different authors are somewhat different, but the general trend of star formation in the unitary comoving volume as a function of redshift, which is often referred to as the ‘Madua diagram/plot’ [139], is likely to be firmly established (see, e.g., Fig. 17).

There are two approaches to constructing this plot. The first relates to a detailed modeling of the star formation history in nearby galaxies using their spectra. The second is more direct and assumes studies of complete samples of galaxies observed at different z . The main problems of this method are relatively small samples of distant galaxies (which is related to the small sizes of deep fields) and poorly known correction for the intrinsic absorption, which can notably reduce the observed luminosity of distant objects. Nevertheless, both approaches yield generally consistent results (see, e.g., [141]).

As seen in Fig. 17, the specific star formation rate rapidly grows from $z = 0$ to $z \sim 1$, has a global maximum at $z \sim 1 - 2$, and then starts decreasing, remaining, however, significant up to the limiting redshift z (~ 6) at which modern estimates are possible. Analysis of the history of star formation in the Universe leads to the conclusion that 50% of all stars existing at $z = 0$ were born at $z \geq 1$, $\sim 25\%$ appeared at $z \geq 2$, $\sim 15\%$ appeared at $z \geq 3$, and $\sim 5\%$ existed already at $z = 5$ [142]. One more important observational result is that the number of massive star systems (with masses exceeding $10^{11} M_{\odot}$) decreases with z , although a small number of such galaxies are also present at $z > 4$ [142].

6. Conclusion

Hundreds of years ago, we inhabited a dwarf Universe consisting of planets and limited by a sphere of fixed stars (Fig. 1). One hundred years ago, the concept of

the Universe consisting entirely of stars dominated. That Universe appeared as a huge oblate star cluster, the Milky Way, with the Sun located close to its center. At the beginning of the third millennium, the volume of the Universe available to astronomical observations includes hundreds of billions of ‘recessing’ galaxies (Fig. 18³), surrounded by dark matter halos and embedded in an anti-gravitating cosmic vacuum [144]. Our Universe has already passed its peak activity and we are living in its history of ‘decline’ when the epoch of active star formation has already ended and galaxies have recessed from each other and only relatively rarely interact with each other.

The sky surveys and selected deep field studies, some of which have been discussed in this review, play a very important role in creating a large-scale picture of the world. Modern sky surveys provide information on the characteristics and spatial distribution of millions of galaxies. Deep fields allow galaxies under formation and their evolution over billions of years to be studied. According to some researchers, should the current progress in observations be continued, the question of the formation and evolution of galaxies will be answered in one or two decades. At that time, we might “look back to this one and recall with nostalgia how exciting it was to help write that story” [145].

The wealth of observational data obtained by the projects described in this review has already been counted in dozens of terabytes. These data, as a rule, are freely accessible and can be used through the world-wide web by both professional researchers and amateurs. All major ground-based telescopes and space observatories also have data archives where results of observations are stored (the BTA observations archive can be found at <http://www.sao.ru>).

The huge available amount of information on the Universe has altered the face of modern astronomy. The current rate of observational data storage on astronomy has reached $\sim 1 \text{ TB/day}$ [146]. Many important tasks, from statistical studies of the Milky Way and studies of the large-scale distribution of galaxies to the discovery of new types of objects, can now be solved without additional observations by telescopes. These new possibilities, which often escape the attention of even professional astronomers, pose ‘technological’ problems, such as rapid and convenient access to world-wide dispersed and often inhomogeneous data, their visualization and analysis, etc. This has stimulated the appearance of the Virtual Observatory concept (<http://www.ivoa.net>) primarily aimed at increasing the efficiency of astronomical studies under conditions of a colossal amount of information [146]. Modern and future multi-wavelength sky surveys create a kind of ‘virtual Universe’ in our computers, and the Virtual Observatory may turn out to be the principal tool for its investigation.

This work is supported by the RFBR grant 03-02-17152.

³ It is instructive to note a certain visual similarity between Fig. 18 and Fig. 1.

Fig. 18. The map of the Universe [143]. An equatorial slice ($-2^\circ < \delta < 2^\circ$) of the galaxy distribution in the sky is presented. The right ascension of objects is plotted along the horizontal axis. The left and right vertical axes show the distance measured in Mpc and in Earth radii, respectively.

References

1. Heninger S.K. *The Cosmographical Glass. Renaissance Diagrams of the Universe* (San Marino, California: The Huntington Library, 1977)
2. Eremeeva A.I. *Vselennaya Gershelya* (Herschel's Universe) (Moscow: Nauka, 1966)
3. Hubble E. *Astrophys. J.* **64** 321 (1926)
4. Hubble E. *Astrophys. J.* **79** 8 (1934)
5. Sandage A., in *The Hubble Deep Field* (Eds M Livio, S M Fall, P Madau) (New York: Cambridge University Press, 1998) p.1
6. Ellis R., in *Galaxies at high redshift. XI Canary Islands Winter School of Astrophysics* (Eds I Pirez-Fournon, M Balcells, F Moreno-Insertis, F Sanchez) (Cambridge: Cambridge Univ. Press, 2003) p.1
7. Hubble E. *Astrophys. J.* **84** 517 (1936)
8. Rosati P., in *Modern Cosmology* (Eds S Bonometto, V Gorini, U Moschella) *Bristol: Institute of Physics Publishing, 2002*, p.312
9. Giavalisco M. *Ann. Rev. Astron. Astrophys.* **40** 579 (2002)
10. Markaryan B.E., Lipovetskii V.A., Stepanyan J.A. *Astrofizika* **15** 549 (1979)
11. Morgan D.H., in *The Future Utilisation of Schmidt Telescopes, ASP Conference Series* **84** 137 (1995)
12. Zwicky F., Herzog E., Wild P., Karpowicz M., Kowal C. *Catalogue of Galaxies and of Clusters of Galaxies: I-IV* (Pasadena: California Institute of Technology, 1961-1968)
13. Vorontsov-Velyaminov B.A., Krasnogorskaya A.A., Arhipova V.P. *Morfologicheskii Katalog Galaktik: I-IV* (Morphological Catalog of Galaxies) (Moscow: Izd. MGU, 1962-1968)
14. Vorontsov-Velyaminov B.A. *Atlas i Katalog Vzaimodeistvuyushchih Galaktik* (Atlas and Catalog of Interacting Galaxies) (Moscow: Izd. MGU, 1959)
15. Karachentsev I.D. *Dvoynye Galaktiki* (Binary Galaxies) (Moscow: Nauka, 1987)
16. Abell G. *Astrophys. J. Suppl.* **3** 211 (1958)
17. Reid I.N., Brewer C., Brucato R.J. et al., *Publ. Astron. Soc. Pacif.* **103** 661 (1991)
18. Maddox S.J., Sutherland W.J., Efstathiou G., Loveday J., *Mon. Not. R. Astron. Soc.* **243** 692 (1990)
19. Maddox S.J., Efstathiou G., Sutherland W.J., Loveday J., *Mon. Not. R. Astron. Soc.* **242** 43P (1990)
20. Dalton G.B., Croft R.A.C., Efstathiou G. et al., *Mon. Not. R. Astron. Soc.* **271** L47 (1994)
21. Pennington R.L., Humphreys R.M., Odewahn S.C. et al., *Publ. Astron. Soc. Pacif.* **105** 521 (1993)
22. Yentis D.J., Cruddace R.G., Gursky H. et al., *Astron. Astrophys. Sci. Lib.* **174** 67 (1992)
23. Hambly N.C., MacGillivray H.T., Read M.A. et al., *Mon. Not. R. Astron. Soc.* **326** 1279 (2001)
24. Lasker B.M., McLean B.J., Shara M.M. et al., *Bull. Inform. CDS* **37** 15 (1989)
25. Postman M., *Publ. Astron. Soc. Pacif.* **106** 108 (1994)
26. Lasker B.M., Doggett J., McLean B. et al., *ASP Conference Series* **101** 88 (1996)
27. Djorgovski S.G., Gal R.R., Odewahn S.C. et al., in *Wide Field Surveys in Cosmology* (Eds S Colombi, Y Mellier) *Gif sur Yvette: Editions Frontiers, 1999*, p.89
28. Skrutskie M.F., Schneider S.E., Stiening R. et al., in *The Impact of Large Scale Near-IR Sky Surveys* (Eds F Garzon et al.) *Dordrecht: Kluwer, 1997*, p.25
29. Jarrett T.H., *Publ. Astron. Soc. Pacif.* **112** 1008 (2000)
30. Jarrett T.H., Chester T., Cutri R. et al., *Astron. J.* **119** 2498 (2000)
31. Jarrett T., *Publ. Astron. Soc. Austr.* **21** 396 (2004)
32. Eichhorn G., *Astron. Geophys.* **45** 3.7 (2004)
33. Colless M., Dalton G., Maddox S. et al., *Mon. Not. R. Astron. Soc.* **328** 1039 (2001)
34. Colless M., Peterson B.A., Jackson C. et al., The 2dF Galaxy Redshift Survey: Final Data Release, 2003; astro-ph/0306581
35. Colless M., in *Measuring and Modeling the Universe* (Ed W L Freedman) *Cambridge: Cambridge Univ. Press, 2004*, p. 196
36. Elgaroy O., Lahav O., Percival W.J. et al., *Phys. Rev. Lett.* **89** 061301 (2002)
37. Percival W.J., Sutherland W., Peacock J.A. et al., *Mon. Not. R. Astron. Soc.* **337** 1068 (2002)
38. Croom S.M., Smith R.J., Boyle B.J. et al. *Mon. Not. R. Astron. Soc.* **349** 1397 (2004)
39. Jones D.H., Saunders W., Colless M. et al., *Mon. Not. R. Astron. Soc.* **355** 747 (2004)
40. Reshetnikov V.P., *Poverhnostnaya Fotometriya Galaktik* (Surface Photometry of Galaxies) (St.Petersburg: Izd. SPbGU, 2003)
41. Lynden-Bell D., Faber S.M., Burstein D. et al., *Astrophys. J.* **326** 19 (1988)
42. York D.G., Adelman J., Anderson J.E. et al., *Astron. J.* **120** 1579 (2000)
43. Stoughton Ch., Lupton R.H., Bernardi M. et al., *Astron. J.* **123** 485 (2002)
44. Abazajian K., Adelman-McCarthy J.K., Agueros M.A. et al., *Astron. J.*, **129** 1755 (2005)
45. Loveday J., *Contemp. Phys.* **43** 437 (2002)
46. Koo D.C., Kron R.G., *Ann. Rev. Astron. Astrophys.* **30** 613 (1992)
47. Sandage A., in *The Deep Universe* (Eds B Binggeli, R Buser) *Berlin: Springer, 1995*, p.1
48. Ellis R.S., *Ann. Rev. Astron. Astrophys.* **35** 389 (1997)
49. Metcalfe N., Shanks T., Campos A. et al., *Mon. Not. R. Astron. Soc.* **323** 795 (2001)
50. McCracken H.J., Shanks T., Metcalfe N. et al., *Mon. Not. R. Astron. Soc.* **318** 913 (2000)
51. Ferguson H.C., Dickinson M., Williams R., *Ann. Rev. Astron. Astrophys.* **38** 667 (2000)

52. Williams R.E., Blacker B., Dickinson M. et al., *Astron. J.* **112** 1335 (1996)
53. Williams R.E., Baum S., Bergeron L.E. et al., *Astron. J.* **120** 2735 (2000)
54. Giaconi R., Zirm A., Wang J.X. et al., *Astrophys. J. Suppl.* **139** 369 (2002)
55. Rosati P., Tozzi P., Giaconi R. et al., *Astrophys. J.* **566** 667 (2002)
56. Alexander D.M., Bauer F.E., Brandt W.N. et al., *Astron. J.* **126** 539 (2003)
57. Barger A.J., Cowie L.L., Capak P. et al., *Astron. J.* **126** 632 (2003)
58. Lehmer B.D., Brandt W.N., Alexander D.M. et al., *Astron. J.* **129** 1 (2005)
59. Heidt J., Appenzeller I., Gabasch A. et al., *Astron. Astrophys.* **398** 49 (2003)
60. Noll S., Mehlert D., Appenzeller I. et al., *Astron. Astrophys.* **418** 885 (2004)
61. Appenzeller I., Bender R., Bohm A. et al., *ESO Messenger* **116** 18 (2004)
62. Kashikawa N., Shimasaku K., Yasuda N. et al., *Publ. Astron. Soc. Japan* **56** 1011 (2004)
63. Maihara T., Iwamuro F., Tanabe H. et al., *Publ. Astron. Soc. Japan* **53** 25 (2001)
64. Taniguchi Y., Ajiki M., Nagao T. et al., *Publ. Astron. Soc. Japan* **57** 165 (2005)
65. Kodama T., Yamada T., Akiyama M. et al., *Mon. Not. R. Astron. Soc.* **350** 1005 (2004)
66. Ouchi M., Shimasaku K., Akiyama M. et al., *Astrophys. J.* **620** L1 (2005)
67. Wolf C., Dye S., Kleinheinrich M. et al., *Astron. Astrophys.* **377** 442 (2001)
68. Wolf C., Meisenheimer K., Rix H.-W. et al., *Astron. Astrophys.* **401** 73 (2003)
69. Kleinheinrich M., Schneider P., Rix H.-W. et al., *Astron. Astrophys.* in press; astro-ph/0412615
70. Wolf C., Meisenheimer K., Kleinheinrich M. et al., *Astron. Astrophys.* **421** 913 (2004)
71. Giavalisco M., Ferguson H.C., Koekemoer A.M. et al., *Astrophys. J.* **600** L93 (2004)
72. Riess A.G., Strolger L.-G., Tonry J. et al., *Astrophys. J.* **607** 665 (2004)
73. Beckwith S., Somerville R., Stiavelli M., *STScI Newsletter* **20** Issue 4 (2003)
74. Bouwens R.J., Thompson R.I., Illingworth G.D. et al., *Astrophys. J.* **616** L79 (2004)
75. Shectman S.A., Landy S.D., Oemler A. et al., *Astrophys. J.* **470** 172 (1996)
76. Arnouts S., D'Odorico S., Cristiani S. et al., *Astron. Astrophys.* **341** 641 (1999)
77. Yee H.K.C., Morris S.L., Lin H. et al., *Astrophys. J. Suppl.* **129** 475 (2000)
78. Drory N., Feulner G., Bender R. et al., *Mon. Not. R. Astron. Soc.* **325** 550 (2001)
79. Cimatti A., Mignoli M., Daddi E. et al., *Astron. Astrophys.* **392** 395 (2002)
80. Davis M., Faber S.M., Newman J.A. et al., *Proc. SPIE* **4834** 161 (2002); astro-ph/0209419
81. Rix H.-W., Barden M., Beckwith S. et al., *Astrophys. J. Suppl.* **152** 163 (2004)
82. Le Fevre O., Mellier Y., McCracken H.J. et al., *Astron. Astrophys.* **417** 839 (2004)
83. Le Fevre O., Vettolani G., Garilli B. et al., *Astron. Astrophys.* (2005); astro-ph/0409133
84. Alcalá J.M., Pannella M., Puddu E. et al. *Astron. Astrophys.* **428** 339 (2004)
85. Karachentsev I.D., *Pis'ma Astron. Zh.* **6** 3 (1980) [Sov. Astron. Lett. **6** 1 (1980)]
86. Fatkhullin T.A., Vasil'ev A.A., Reshetnikov V.P. *Pis'ma Astron. Zh.* **30** 323 (2004) [Astron. Lett. **30** 283 (2004)]
87. Sandage A., *Astrophys. J.* **133** 355 (1961)
88. Nagashima M., Yoshii Y., Totani T., Gouda N., *Astrophys. J.* **578** 675 (2002)
89. Gardner J.P., *Publ. Astron. Soc. Pacif.* **110** 291 (1998)
90. Peebles P.J.E. *The Large-Scale Structure of the Universe* (Princeton, NJ: Princeton University Press, 1980)
91. Maller A.H., McIntosh D.H., Katz N., Weinberg M.D., *Astrophys. J.* **619** 147 (2005)
92. Jones B.J.T., Martinez V.J., Saar E., Trimble V., *Rev. Mod. Phys.* **76** 1211 (2004)
93. Budavari T., Connolly A.J., Szalay A.S. et al., *Astrophys. J.* **595** 59 (2003)
94. Maroto A.L., Ramirez J., astro-ph/0409280
95. Tegmark M., Blanton M.R., Strauss M.A. et al., *Astrophys. J.* **606** 702 (2004)
96. Kraan-Korteweg R.C., *Rev. Mod. Astron.*, in press; astro-ph/0502217
97. Frith W.J., Buswell G.S., Fong R. et al., *Mon. Not. R. Astron. Soc.* **345** 1049 (2003)
98. Stiavelli M., Djorgovski S.G., Pavlovsky C. et al., *Astrophys. J.* **622** L1 (2005)
99. Miller L., Croom S.M., Boyle B.J. et al. *Mon. Not. R. Astron. Soc.* **355** 385 (2004)
100. Schechter P., *Astrophys. J.* **203** 297 (1976)
101. Norberg P., Cole Sh., Baugh C.M. et al., *Mon. Not. R. Astron. Soc.* **336** 907 (2002)
102. Croton D.J., Farrar G.R., Norberg P. et al. *Mon. Not. R. Astron. Soc.* **356** 1155 (2005)
103. Gabasch A., Bender R., Seitz S. et al., *Astron. Astrophys.* **421** 41 (2004)
104. Fried J.W., von Kuhlmann B., Meisenheimer K. et al., *Astron. Astrophys.* **367** 788 (2001)
105. Pozzetti L., Cimatti A., Zamorani G. et al., *Astron. Astrophys.* **402** 837 (2003)
106. Rudnick G., Rix H.-W., Franx M. et al. *Astrophys. J.* **599** 847 (2003)
107. Reshetnikov V.P., Sotnikova N.Ya. *Astrofizika* **36** 435 (1993) [Astrophysics **36** 265 (1994)]
108. Karachentsev I.D., Makarov D.I., in *Galaxy Interactions at Low and High Redshift* (Eds J E Barnes, D B Sanders) *Dordrecht: Kluwer Acad. Publ.*, 1999, p.109
109. Abraham R.G., Tanvir N.R., Santiago B.X. et al., *Mon. Not. R. Astron. Soc.* **279** L47 (1996)
110. Conselice Ch.J., Bershady M.A., Jangren A., *Astrophys. J.* **529** 886 (2000)
111. Reshetnikov V.P., *Astron. Astrophys.* **353** 92 (2000)

112. Conselice Ch.J., Bershadsky M.A., Dickinson M., Papovich C., *Astron. J.* **126** 1183 (2003)
113. Hibbard J.E., Vacca W.D., *Astron. J.* **114** 1741 (1997)
114. Elmegreen B.G., Elmegreen D.M., Hirst A.C., *Astrophys. J.* **612** 191 (2004)
115. Jogee Sh., Barazza F.D., Rix H.-W. et al., *Astrophys. J.* **615** L105 (2004)
116. Lilly S., Schade D., Ellis R. et al., *Astrophys. J.* **500** 75 (1998)
117. Barden M., Rix H.-W., Somerville R.S. et al., *Astrophys. J.*, in press; astro-ph/0502416
118. Ziegler B.L., Bohm A., Fricke K.J. et al., *Astrophys. J.* **564** L69 (2002)
119. Reshetnikov V., Battaner E., Combes F., Jimenez-Vicente J., *Astron. Astrophys.* **382** 513 (2002)
120. Reshetnikov V.P., Dettmar R.-J., Combes F., *Astron. Astrophys.* **399** 879 (2003)
121. Kobulnicky H.A., Kewley L.J., *Astrophys. J.* **617** 240 (2004)
122. van der Wel A., Franx M., van Dokkum P.G., Rix H.-W., *Astrophys. J.* **601** L5 (2004)
123. Holden B.P., van der Wel A., Franx M. et al., *Astrophys. J.* **620** L83 (2005)
124. Treu T., in *Clusters of Galaxies: Probes of Cosmological Structure and Galaxy Evolution* (Eds J S Mulchaey, A Dressler, A Oemler) *Cambridge: Cambridge Univ. Press, 2004*, p.178
125. Stern D., Spinrad H., *Publ. Astron. Soc. Pacif.* **111** 1475 (1999)
126. Fan X., Strauss M.A., Schneider D.P. et al., *Astron. J.* **125** 1649 (2003)
127. Dey A., Spinrad H., Stern D. et al., *Astrophys. J.* **498** L93 (1998)
128. Spinrad H., astro-ph/0308411
129. Reshetnikov V.P., Vasil'ev A.A. *Pis'ma Astron. Zh.* **28** 3 (2002) [*Astron. Lett.* **28** 1 (2002)]
130. Ouchi M., Shimasaku K., Furusawa H. et al., *Astrophys. J.* **582** 60 (2003)
131. Ouchi M., Shimasaku K., Okamura S. et al., *Astrophys. J.* **611** 685 (2004)
132. Ferguson H.C., Dickinson M., Giavalisco M. et al., *Astrophys. J.* **600** L107 (2004)
133. Bouwens R.J., Illingworth G.D., Blakeslee J.P. et al., *Astrophys. J.* **611** L1 (2004)
134. Gunn J.E., Peterson B.A., *Astrophys. J.* **142** 1633 (1965)
135. Loeb A., Barkana R., *Ann. Rev. Astron. Astrophys.* **39** 19 (2001)
136. Becker R.H., Fan X., White R.L. et al., *Astron. J.* **122** 2850 (2001)
137. Sazhin M.V. *Usp. Fiz. Nauk* **174** 197 (2004) [*Phys. Usp.* **47** 187 (2004)]
138. Wyithe J.S., Loeb A. *Astrophys. J.* **586** 693 (2003)
139. Madau P., Ferguson H.C., Dickinson M.E. et al. *Mon. Not. R. Astron. Soc.* **283** 1388 (1996)
140. Bouwens R.J., Illingworth G.D., Thompson R.I. et al. *Astrophys. J.* **606** L25 (2004)
141. Heavens A., Panter B., Jimenez R., Dunlop J. *Nature* **428** 625 (2004)
142. Drory N., Salvato M., Gabasch A. et al. *Astrophys. J.* **619** L131 (2005)
143. Gott J.R., Juric M., Schlegel D. et al. *Astrophys. J.* **624** 463 (2005)
144. Chernin A.D. *Usp. Fiz. Nauk* **171** 1153 (2001) [*Phys. Usp.* **44** 1099 (2001)]
145. Fall S.M., in *Building Galaxies: from the Primordial Universe to the Present* (Eds F Hammer, T X Thuan, V Cayatte et al.) *XXX: World Scientific Publishing, 2000*, p.463
146. Djorgovski S.G., Williams R. astro-ph/0504006

Translated by K.A. Postnov; edited by A.M. Semikhatov

This figure "fig4.jpg" is available in "jpg" format from:

<http://arxiv.org/ps/astro-ph/0603154v1>

This figure "fig13.jpg" is available in "jpg" format from:

<http://arxiv.org/ps/astro-ph/0603154v1>

This figure "fig18.jpg" is available in "jpg" format from:

<http://arxiv.org/ps/astro-ph/0603154v1>